DALHOUSIE UNIVERSITY

Theoretical Descriptors of Electrides

Stephen G. Dale* and Erin R. Johnson*

Department of Chemistry, Dalhousie University, 6274 Coburg Rd, P.O.Box 15000 B3H 4R2, Halifax, Nova Scotia, Canada

E-mail: stephen.dale@dal.ca; erin.johnson@dal.ca

Abstract

Electrides are ionic substances in which the anionic species is stoichiometrically replaced with localized electrons that reside within crystal voids. Originally discovered in 1983, the past decade has seen a sharp rise in the number of known electride materials, most notably the isolation of the first air- and water-stable electride. As the presence of localized interstitial electrons cannot be directly detected experimentally, researchers have turned to density-functional theory (DFT) to discover new electrides. In this work, we survey eight common theoretical descriptors of electrides for their efficacy in identifying these materials. Illustrative examples are presented for all classes of electrides: organic, inorganic, 2D, elemental, and molecular electrides. In general, density-based descriptors such as the electron localisation function (ELF) and localized-orbital locator (LOL) are shown to be the most consistently reliable. Limitations of DFT treatments of electrides are also discussed.

*To whom correspondence should be addressed

Dr. Stephen G. Dale is a postdoctoral researcher at Dalhousie University under the supervision of Prof. Axel D. Becke. His research focuses on the development of density-functional theory (DFT) and its applications in the discovery and characterisation of new materials. Stephen obtained his B.Sc. (1st Hons.) from the University of Western Australia and was introduced to research by Dr. Duncan A. Wild in the form of Time-of-Flight Photoelectron Spectroscopy. In 2017, he received his Ph.D. from the University of California, Merced under the supervision of Prof. Erin R. Johnson. His thesis work focussed on understanding of the electride materials using DFT methods, which remains an ongoing research interest.

Dr. Erin R. Johnson is a full Professor at Dalhousie University, where she holds the Herzberg-Becke Chair in Theoretical Chemistry. Her research focuses on development and applications of density-functional theory, with an emphasis on intermolecular interactions. Notable methods co-developed by Johnson include the exchange-hole dipole moment dispersion model, non-covalent interactions analysis, and the Becke-Johnson exchange potential. Erin obtained her B.Sc. (Hons.) from Carleton University, conducting research in the group of Dr. Gino A. DiLabio. She completed her Ph.D. in chemistry at Queen's University in 2007, under the supervision of Prof. Axel D. Becke. This was followed by an NSERC post-doctoral fellowship at Duke University in the group of Prof. Weitao Yang. She held her first faculty position at the University of California, Merced, from 2010-2015, before returning to Canada. She was awarded the 2018 Dirac Medal by the World Association of Theoretical and Computational Chemists.

1 Introduction

The presence of localized, interstitial electrons defines the unusual electronic structure of the electrides and gives these materials unique chemical properties,[1] most notably the ability to act as very strong and selective reducing agents.[2–5] Electrides are beginning to find use in modern technological applications, such as the development of organic light-emitting diodes,[6] exotic ion generation,[7] improved catalysts for CO_2[8] and N_2[9–11] splitting, more efficient cathodes for electrochemical reactions,[12] and new potential super-conductors.[13] As a result, recent years have seen a veritable explosion in electride research from the perspectives of both experiment and theory, with the first two-dimensional (2D) electride and first water-stable electride being reported in 2013[14] and 2016,[11] respectively.

The initial discovery of electrides was a consequence of research into solvated-electron chemistry. First observed to form from solutions of alkali metals in ammonia by Sir Humphry Davy in 1808,[15] the concept of a solvated electron as an independent species in solution was later introduced by Charles A. Kraus.[16] James L. Dye, arguably the father of electrides, began work on metal-ammonia solutions in 1954. Introduction of electron-rich ligands, such as crown ethers[17] and cryptands,[18] facilitated the precipitation of a solid phase from solvated-electron solutions. In 1974, Dye *et al.*[19] synthesised the first alkalide crystal, Na^+(cryptand-2.2.2)Na^-. The alkalides are materials which contain negatively charged alkali metal atoms and are closely related to the electrides.[1,20,21] The first electride, $Cs^+(18C6)_2e^-$, was produced by Dye's group in 1983[22] and its crystal structure identified in 1986.[23]

Since this time, six additional organic electrides, consisting of alkali metals complexed to crown ether or cryptand ligands, have been synthesised and characterised.[24–30] This was followed by the isolation of the first inorganic electride, $[Ca_{24}Al_{28}O_{64}]^{4+}(4e^-)$, in 2003 by Matsuishi *et al.*[31] In 2009, researchers also identified a previously predicted[32] electride phase of sodium under extremely high pressure.[33] Since 2013, the field has seen a significant acceleration in the rate of electride discovery and variety, with the characterisation of eight additional inorganic electrides,[11,34–38] including the 2D layered electrides, $[Ca_2N]^+e^-$ and

$[Y_2C]^+e^-$.[14,39]

Definition: An electride is an ionic substance in which the anionic species is a stoichiometrically localized electron.

Problem: To date, the presence of localized electrons can only be inferred from experimental results, not directly measured.

With the increasing breadth of the electride field, an important question remains: How does one define and identify an electride? While a functional definition for an electride is provided in the first sentence of this article, in practice the direct observation of the localized electron species inside a crystal void is currently impossible and the location of the anionic species can only be inferred from the experimental results. Consequently, theoretical methods, which do not suffer from these experimental challenges, have heavily supplemented the ongoing investigation and understanding of electrides. This article seeks to examine the research efforts to date applying electronic-structure theory to characterise the electride materials, including a brief history of the field. Possible criteria for identification of a particular material as an electride will be highlighted and discussed. The generality and transferability of each putative criteria will be ascertained through illustrative examples from each general class of electride: organic, inorganic, 2D, elemental, and molecular electrides.

2 Organic Electrides

2.1 Initial experimental characterisation

To date, seven organic electrides have been discovered and characterised, primarily by the Dye lab and their collaborators: $Cs^+(18C6)_2e^-$,[22,23] K^+(cryptand-2.2.2)e^-,[24,40] $Cs^+(15C5)_2e^-$,[41] $[Cs^+(15C5)(18C6)e^-]_6(18C6)$,[27] Li^+(cryptand-2.1.1)e^-,[28] Rb^+(cryptand-2.2.2)e^-,[29] and Na^+(tripip-aza-2.2.2)e^-.[30] Regarding this notation, all electrides discussed in this article are represented with the chemical formula of the crystal framework, followed by the number of

localized electrons associated with that chemical formula. The unit cell of the simplest organic electride, $Cs^+(15C5)_2e^-$, is shown in Figure 1. In the electride literature, the notation mCn is commonly used to represent crown ether molecules, where m refers to the total number of atoms and n refers to the number of oxygen atoms in the ring. The primary barrier to synthesis and characterisation of the organic electrides is their inherent instability, readily reacting with impurities throughout production or decomposing at elevated temperatures (all organic electrides decompose between 240[42] and 283 K[30]).

The X-ray crystallographic structures[24–30] reveal that there is one or more clear crystal void(s) in each of the organic electrides, with diameters of $0.4 - 0.6$ nm. This suggests the presence of crystal voids as the first potential descriptor for identification of electride materials. The impact of crystal void topology on the electronic and magnetic properties of the electrides was extensively investigated by Dye *et al.* in 1996.[43] The surface created by the van der Waals radii of the atoms was used to map the location and sizes of crystal voids within the organic electrides of known crystal structure. By assuming that the extra electron is localized within these regions, it was then possible to loosely link the size and proximity of the crystal voids to the magnetic susceptibility maxima and conductivity measurements. Additionally, our own work[44] used analysis of the procrystal density[45,46] as an alternative technique to map the electride crystal voids. The procrystal density is the sum of all the atomic densities within a crystal structure. A procrystal surface, plotted at a deliberately small isodensity value, allows for easy identification of crystal voids and an example of this for the $Cs^+(15C5)_2e^-$ electride is provided in Figure 1(c). However, the presence of a void within a crystal does not mean that it will be occupied by a localized electron, as porous materials such as zeolites and metal-organic frameworks are not electrides. Even for the $[Cs^+(15C5)(18C6)e^-]_6(18C6)$ electride,[27] density-functional theory (DFT) calculations have shown that not all of the crystal voids are occupied by the interstitial electrons.[44]

1 - Property: Void spaces must be present within an electride crystal if an electron is to exist independent of any atomic species.

Problem: The existence of a void space does not ensure that an electron is localized within it.

With the exception of the theoretical analysis of the crystal voids, the majority of computational studies on these materials have focused on confirming their electride nature. The experimental case for the presence of localized interstitial electrons is based primarily on NMR data. The ^{133}Cs NMR spectra of $Cs^+(18C6)_2e^-$ and $Cs^+(15C5)_2e^-$ were recorded in 1987 and 1991, respectively, by Dawes *et al.*[41,47] The purpose of these measurements was to demonstrate the presence of a cationic caesium metal species and, by process of elimination, infer the existence of the localized electron. The Knight shift was used to determine the spin density of the caesium species as 0.063% and 0.003% of that observed in free atomic caesium for $Cs^+(15C5)_2e^-$ and $Cs^+(18C6)_2e^-$, respectively. These values were then compared to data for the analogous alkalide species,[47–55] where NMR had previously confirmed the presence of negatively charged alkali metal atoms occupying the same lattice sites as the electride crystal voids. As the spin density depletion of the caesium species matched that observed for the alkalides, it was argued that the excess electron must localize within the crystal void. These NMR spectra were then used as reference values for theoretical investigations of electrides which attempted to justify or refute the presence of localized electrons.

Golden *et al.*[56] analysed optical adsorption and NMR spectral data to determine upper and lower bounds to the 6*s* electron density maximum in order to estimate its spatial distribution. This work concluded that the experimental spectra were consistent with the electron being localized about the caesium nucleus. At odds with this conclusion is the work of Rencsok *et al.*,[57] who attempted to explain the experimental NMR results using a simple charged-shell model of the potential experienced by the caesium 6*s* electron when complexed to the crown ethers. The effect of this potential is to shift the 6*s* electron density maximum

outwards from the caesium nucleus, which could account for the observed spin-density depletion. Based on this result, they argued that the valence electron of caesium, while still centralised around the caesium atom, will isolate the charge at the outside of the encapsulating ligands. This sparked a debate in the literature,[58,59] but this series of papers resulted in no clear conclusion without more spectral information to differentiate between the two opposing models.

2.2 Electronic structure of bulk electrides

The early theoretical investigations of electrides focused on a simplified model system, $Li^+(9C3)_2e^-$, to reduce the computational cost. Additionally, calculations were only feasible for a single complex, rather than the periodic solid. The first such study was conducted by Rencsok *et al.*[57] using Hartree-Fock (HF) calculations with extremely small basis sets (STO-3G, 3-21G, and 6-31G). Mulliken population analysis showed a decrease in spin density of the Li and increased negative charge on the O atoms in the complex, relative to the separated, neutral species. The authors argued that, for the solid material, the valence electron of the alkali metal is not present in the crystal voids, but is instead "squeezed to the outside of the large molecule." However, a subsequent study by the same group using the larger 6-31++G* basis set showed that the valence electron of lithium is located predominantly outside the complex in a Rydberg-like state,[60] supporting the localized electron-in-a-void model. However, the major flaw in this approach is that single-molecule calculations will not reflect the electronic structure of the real, condensed-phase electride. Solid-state calculations will be considered in the remainder of this section and have provided compelling evidence for the localized-electron picture.

In 1990, Allan *et al.*[61] conducted Hartree-Fock calculations within the tight-binding approximation[62] on a single unit cell of $Cs^+(18C6)_2e^-$. Minimal basis sets were used, with an extra set of *s* functions located at the centre of the crystal void. It was found that the potential experienced by the electride electron was repulsive at the caesium atom and attractive

near the void. This model also reproduced the optical absorption spectrum of the electride and the spin-density deficiency at the caesium atom observed in the NMR experiments. While it was not explicitly pointed out, it is also worth mentioning that the density of states of the extra *s* 'orbital' showed a peak at the Fermi level, consistent with later studies.

In 1993, Singh *et al.*[63] conducted local density approximation (LDA) calculations using a mixed-basis method on $Cs^+(15C5)_2e^-$ in order to investigate the band structure, electron density, and chemical potential of the electride. Singh *et al.* found a high lying "electride" state in the band structure which, when visualised, was clearly localized within the crystal void. The chemical potential of the void region was shown to be higher than that of the surrounding crystal and localisation of the electron in this region was justified by a need to lower its kinetic energy. This is due to the required orthogonality of the electride state with the bonding states surrounding the molecules. In order for the electron to exist near the alkali metal-ligand complexes, it would need to occupy a much higher energy state than the one corresponding to the centre of the crystal void.

2 - Property: The 'electride state' is a high-lying, partially occupied valence state in the band structure of an electride, the density of which is localized within the crystal void.

Problem: Inorganic electrides are more metallic in nature and the electride state is difficult to isolate in these cases.

After this initial discourse regarding the location of the localized electron in the early 1990's, theoretical work on the organic electrides tapered off due to the computational challenges. It was not until the present decade that calculations of a full electride crystal were revisited. Before discussing the results of periodic-boundary DFT calculations, we will briefly note some general trends in the behaviour of various levels of density-functional approximations. The vast majority of DFT calculations on crystalline electrides have been performed with the local density approximation (LDA) or generalised gradient approximation (GGA) functionals, such as PBE[65] or B86bPBE,[64,65] with or without dispersion corrections. These

Figure 1: Computed properties of the $Cs^+(15C5)_2e^-$ electride: a) the unit-cell geometry; b) the band structure; c) the procrystal density, showing a 0.001 au isosurface; d) the density of the 'electride' band ($-1 < E < 0$ eV), showing a 0.0006 au isosurface; e) the reduced density gradient used in NCI, showing a 0.5 au isosurface; f) the ELF, showing a 0.5 au isosurface; g) the LOL, showing a 0.5 au isosurface. All 2D plots map onto the $(0\bar{1}1)$ plane. The calculations used B86bPBE-XDM[64–66] with plane-wave and density-expansion cut-offs of 100 and 1000 Ry, and a $4 \times 4 \times 4$ k-point mesh. The crystal structure was obtained from the work of Dawes *et al.*[41,67]

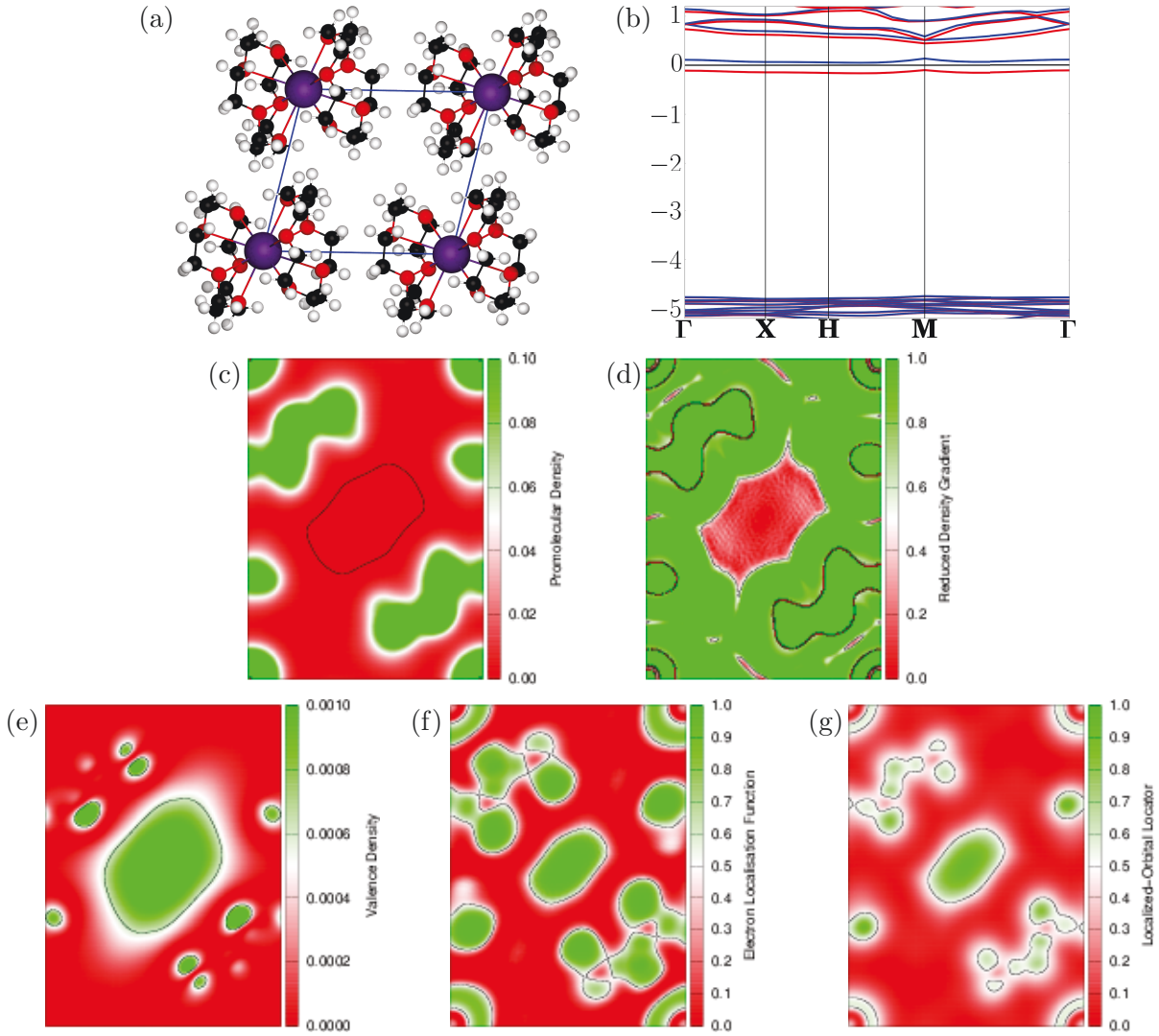

functionals are by far the most widely used due to their computational efficiency for plane-wave calculations. However, due to their inherent delocalization error,[68–79] they will tend of overly delocalize the density distribution of the excess electron[75,80,81] and consequently

underestimate the magnitude of the charge for the interstitial anionic sites. These functionals also tend to underestimate the band gaps of semi-conductors,[82–85] causing them to insufficiently isolate the electride state from the lower-lying valence bands. Conversely, hybrid functionals such as HSE[86] or B3LYP,[87] will reduce delocalization error, better localize the interstitial electrons, and improve the prediction of the band structure. However, due to their high computational cost, these methods are applicable to only the smallest known electrides."

In 2014, we conducted periodic-boundary, planewave/pseudopotential DFT calculations on all the existing electrides (8 at that time).[44] In agreement with the findings of Singh *et al.*, an electride state was identified in evey case. As an example, the band structure of $Cs^+(15C5)_2e^-$ is presented in Figure 1(b). The electride state is separated from the valence and conduction bands and is half occupied. The density of the electride state is localized in the crystal voids, as shown in Figure 1(c). The existence of this electride state constitutes our next well defined property that can be tested computationally to identify electride crystals. DFT calculations can readily, and reliably, identify the electride state of the organic electrides. However, for the inorganic electrides, we will see later that this state is often overlapping with others in the conduction or valence bands and, consequently, can be difficult to identify. Further, the presence of an electronic band between the valence and conduction bands is not a unique phenomenon and is commonly termed a mid-band state in other materials.[88] The density of this state can either localize on atomic centers or, in the case of an F-center defect,[89] not be stoichiometric, so that materials exhibiting such mid-band states are not necessarily electrides.

In addition to demonstrating the consistent occurrence of the electride state, our 2014 work also introduced a number of new density analysis methods to the electride field, including the quantum theory of atoms-in-moleules (QTAIM)[90–93] and non-covalent interaction (NCI) plots.[94–96] QTAIM defines atoms as regions of electron density isolated by zero-gradient isosurfaces; this allows for density maxima to be found that are not associated

with an atomic centre. The interstitial electrons in the organic electrides possess their own non-nuclear maxima (NNMs) in the electron density, which is another potential identifier of electride crystals. The DFT calculations reliably identified NNMs for all of the organic electrides. The charge for each of these interstitial anionic sites can be computed by integration of the electron density over the entire QTAIM basin corresponding to the non-nuclear density maximum. In practise, this was achieved using the Yu-Trinkle algorithm,[97] as implemented in the Critic2 program.[98] For all of the organic electrides, these anionic sites were found to possess a significant fraction of localized charge, in excess of 0.1 e^-.[44] The prediction of a fractional charge is consistent with the expected diffuse nature of the localized electron, overlapping with the electron density of the neighbouring atoms. However, this diffuse nature will be exacerbated by errors in local density functionals that tend to excessively delocalize electron density and over-stabilise fractional charges.[68–79] A further complication with using NNMs as a descriptor is that they are not present or are extremely difficult to identify for the inorganic electrides. The crystal voids within which the electrons localize are much smaller in inorganic materials; this causes increased overlap of the electron density with that of the neighbouring atoms, obscuring any NNMs that might form. Finally, NNMs are not necessarily indicators of electrides as they are predicted to exist in other solids, particularly for ionic crystals with F-centre defects[99–101] (where the presence of the NNM is not stoichiometric), and even in small molecules, such as Li_2.[102,103]

3 - Property: The localized electrons can be identified as NNMs in the electron density using QTAIM analysis.
Problem: NNMs are not present for the inorganic electrides and the presence of a NNM does not guarantee that a given material is an electride.

NCI plots display isosurfaces with low reduced electron-density gradient, in regions of low density.[94] They are typically used for identifying non-covalent interactions, such as hydrogen-bonding, halogen-bonding, and π-stacking, in real-space. NCI plots also allow visualisation of localized electrons within crystal voids, as these regions possess a slowly-varying density and,

consequently, a low reduced density gradient. An example NCI plot for the $Cs^+(15C5)_2e^-$ electride is provided in Figure 1(d). NCI plots can be viewed as an extension of QTAIM, in that the isosurfaces enclose all the zero-gradient critical points with sufficiently low density, including NNMs. However, because the isosurfaces are based on low, but not zero, reduced gradient, the presence of a NNM is not strictly required to allow visualisation of interstitial electrons. As a result, NCI plots can even depict the localized electrons in an inorganic electride where no NNMs are present.[44] We note that, for cases where an unoccupied cage is present in the structure, there may still be a very small region at its centre with near-zero reduced density gradient (a cage critical point in QTAIM). However, this situation will stand in sharp contrast to appearance of interstitial electrons, when the NCI isosurfaces enclose much larger volumes, in which the electron density is very slowly varying; this was illustrated previously[44] for the unoccupied void in the $[Cs^+(15C5)(18C6)e^-]_6(18C6)$ electride.[27]

4 - Property: NCI plots can be used to identify extensive regions with low reduced density gradients corresponding to the localized interstitial electrons.
Problem: It can be difficult to visually distinguish isosurfaces enclosing the localized electrons from the many other diverse types of interactions appearing in NCI plots.

2.3 Magnetic properties of electrides

The unusual electronic structure of the organic electrides causes these materials to have an anti-ferromagnetic ground state. The magnetic susceptibility as a function of temperature has been measured for all of the organic electrides, and consistently shows anti-ferromagnetic character at low temperatures and Curie-Weiss behaviour at higher temperatures.[21,28–30,41,104,105] In 1997, Dye[104] investigated the magnetic properties of the five known electrides (at that time) using a model Heisenberg Hamiltonian, which describes the spin-spin interactions between electrons at neighbouring sites in a dimer or lattice. Provided the chosen model Hamiltonian reproduces the crystal geometry, it can reliably describe the

coupling between the unpaired interstitial electrons and predict the magnetic susceptibility behaviour. Assuming 1D coupling through only the largest channels, the model Heisenberg Hamiltonian predicted a linear correlation between the logarithm of the spin coupling constant of each electride and the cross-sectional area of the channels linking the crystal voids, evaluated using the atomic van der Waals radii.[43]

In 2011, Ryabinkin *et al.*[106] used a 'dog-bone' shaped cavity model to establish a more specific rule for the dependence of the magnetic coupling on the cross-sectional area of the electrides' cavities and channels. The dog-bone consists of two spheres to represent the interstitial cavities, connected by a thin cylinder to represent the coupling channels. Two electrons are confined within this potential well and their interaction is modelled with an exact two-electron Hamiltonian.[107,108] This study found a more complex, but much stronger, relationship between the coupling constant and the cross-sectional areas and channel length used to define the dog-bone potential. However, being strictly 1D, the dog-bone model is only valid for electrides that exhibit quasi-1D electron-electron coupling. As such, it is not applicable to electrides like K^+(cryptand-2.2.2)e^-, which exhibits a strong 2D channel structure,[104] or $[Cs^+(15C5)(18C6)e^-]_6(18C6)$, in which the coupling occurs around a six-membered ring.[109]

In 2016, spin-polarised DFT calculations were able to characterise the ferromagnetic and anti-ferromagnetic states of six of the seven known organic electrides.[110] The anti-ferromagnetic state was correctly predicted to be the more stable in all cases. Consistent with the assumptions of Dye[104] and Ryabinkini *et al.*,[106] spin-density plots demonstrated that the magnetic properties of the electride crystals indeed originate from the localized electron at the centre of the crystal voids; this represents another descriptor of the electride crystals. Further, by assuming an infinite 1D Heisenberg Hamiltonian, it was possible to calculate spin coupling constants for these electrides. However, a limitation of this analysis is that the chosen 1D Heisenberg Hamiltonian does not necessarily reflect the true behaviour of the coupling in a given electride crystal. The most obvious exam-

ple of this is $[Cs^+(15C5)(18C6)e^-]_6(18C6)$, for which previous modeling required the use of a six-membered Heisenberg ring Hamiltonian.[109] Additionally, the magnetic states of K^+(cryptand-2.2.2)e^- could not be converged with these spin-polarised DFT calculations.

5 - Property: The magnetic properties of the electride crystals originate from the unpaired, interstitial electrons.
Problem: Only the organic electrides have unpaired electrons and possess measurable magnetic properties; most of the inorganic electrides have only paired electrons.

An attempt to move away from the 1D Heisenberg Hamiltonian was presented by Kim *et al.*,[111] who used magnetic-force linear-response theory (MFT) to calculate the coupling constants of all relevant pairwise interactions within the electride crystals. This work showed that the magnetic coupling regime for four of the electrides, K^+(cryptand-2.2.2)e^-, $[Cs^+(15C5)(18C6)e^-]_6(18C6)$, Li^+(cryptand-2.1.1)e^-, and Rb^+(cryptand-2.2.2)e^-, is indeed long range and not appropriately modelled by a 1D Hamiltonian. Further, this methodology was able to model successfully the anti-ferromagnetic state of K^+(cryptand-2.2.2)e^-.

Most recently, a pressure-induced anti-ferromagnetic to ferromagnetic transition of $Cs^+(15C5)_2e^-$ was theoretically predicted at 3 GPa by Dale *et al.*[112] Using current technology, this prediction is readily accessible for experimental testing. If verified, this could represent a new direction for technological development of electrides.

2.4 Thermochemistry of electride formation

Finally, it is worth reviewing the rationale behind the synthesis of Na^+(tri-pip-aza-2.2.2)e^- in more detail. This was the first room-temperature-stable organic electride, designed by Redko *et al.* using theoretical calculations to inform experiment.[30] Organic electrides have two modes of decomposition: reduction of the cryptand/crown ether ligand by the solvated electron and de-coordination of the metal from the cage ligands. If a cage ligand with nitrogen, rather than oxygen, branches is used, then the reductive decomposition occurs at a

higher temperature. However, this also reduces the metal-ligand binding energy and causes the second mode of decomposition to occur at a lower temperature. To optimise stability, a number of nitrogen-based cage complexes were selected and their binding energies to the sodium cation calculated using B3LYP/6-311+G(d).[87] The oxygen-containing cryptand-2.2.2, shown on the left of Figure 2, had previously been used in electride synthesis and gives the largest metal-ligand binding energy. However, due to the presence of oxygen, it is vulnerable to reduction by the localized electrons. The remaining cryptands in Figure 2 were proposed complexing ligands, with the right-most predicted to give the highest binding energy of the nitrogen-only cryptands. This ligand was then successfully used in the synthesis of the first room-temperature-stable organic electride. This work gives us another property necessary for synthesis of an electride, namely a strong metal-ligand binding energy for the cationic complex.

Figure 2: Structures of the ligands considered for use in synthesis of the first room-temperature-stable organic electride.[30] From left to right, the ligands are cryptand-2.2.2, permethylated-peraza-2.2.2, and tri-pip-aza-2.2.2.

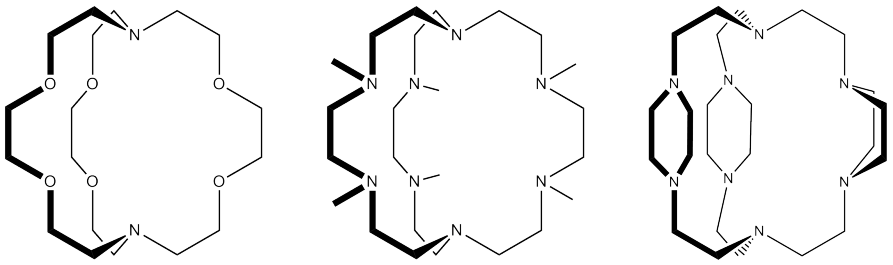

6 - Property: To form an electride, a alkali metal complex must have a low ionization potential and the resulting cation must have a high metal-ligand binding energy.
Problem: Only the organic electrides are composed of alkali metal complexes.

In 2017 Dale *et al.*[113] constructed thermodynamic cycles for the alkali metal-ligand complexes that are the building blocks of the organic electrides. This work reinforced the conclusion of Redko *et al.*,[30] showing that all the existing electride (and alkalide) materials possess

strong metal-ligand binding energies. Further, it was found that the component alkali-metal complexes all possess an ionization potential (IP) in the range of 1-2 eV. This also suggests that a specific, consistently-low IP may be necessary for the formation of stable electride materials.

As the initial electrides to be discovered, the organic electrides establish a baseline of characteristic properties for this entire class of materials. However, as we discuss the diversity of more recent electride discoveries, we will see that these properties are not necessarily general.

3 Inorganic Electrides

In the new millennium, the focus of both theoretical and experimental work shifted to finding an inorganic electride. The first attempts involved doping zeolite crystals with alkali metals that would bind to the natural pores of the crystal structure.[114] While having similar properties to electrides, this style of crystal is not strictly an electride, as the electrons released into the crystal from the alkali atoms remain localized near the parent metal.[115–118]

3.1 The calcium-aluminium electride

The first successful production of an inorganic electride, $[Ca_{24}Al_{28}O_{64}]^{4+}(4e^-)$, was in 2003 by Matsuishi *et al.*[31] Studies of $[Ca_{24}Al_{28}O_{64}]^{4+}(4e^-)$ constitute by far the largest portion of electride research for any single material.[2,6,7,9,10,12,13,31,44,119–130] Its crystal structure is identical to that of the $[Ca_{24}Al_{28}O_{64}](2O^{2-})$ calcium cement, originally characterised in 1970,[131] with the oxide anions replaced with localized electrons. Contrary to the electrides considered so far, this material has only one localized electron evenly distributed over three voids (or cages) within the crystal; however, while not 1:1, this ratio is still stoichiometric.

$[Ca_{24}Al_{28}O_{64}]^{4+}(4e^-)$ has a decomposition temperature of 1600°C,[119] and is atmospherically stable up to 300°C,[120,121] making it considerably more stable than the organic electrides.

For comparison, Na^+(tri-pip-aza-2.2.2)e^- possesses a decomposition temperature of 110 °C,[30] the highest of the organic electrides. The greater stability of $[Ca_{24}Al_{28}O_{64}]^{4+}(4e^-)$ allows for a much more detailed investigation of this electride's properties and applications.[2,6,7,9,10,12] A number of interesting properties have been observed, including anti-ferromagnetism,[31] an insulator-metal transition,[122] a superconducting transition at 0.2 K,[13] and an intermediate work function of 2.4 eV, typical of semi-conducting materials.[120,121]

After the initial discovery of $[Ca_{24}Al_{28}O_{64}]^{4+}(4e^-)$, a theoretical study by Sushko *et al.* quickly followed.[123] This work used an embedded cluster model consisting of two (inequivalent) cages cut from the crystal, treated using the B3LYP density functional,[87] surrounded by 64 unit cells treated classically.[132] The highest occupied molecular orbital and lowest unoccupied molecular orbitals (HOMO and LUMO) were found to be localized within opposite cages, with the excitation energy of the resulting inter-cage hopping falling in the IR range. Higher excited states showed intra-cage shifts of the electron density, with energies in the UV range, consistent with absorption spectra of the inorganic electride.[124]

In 2004, two studies by Medvedeva *et al.*[125,126] computed the band structures of the $[Ca_{24}Al_{28}O_{64}]^{4+}(4e^-)$ electride and its hydrogen-doped equivalent. These works used the linear muffin-tin orbital (LMTO) method and the atomic-sphere approximation,[133] with oxygen-like orbitals included at the centre of each cage to allow for electron localisation. Both crystals showed electronic states near the Fermi level, typical of electrides. However, no significant charge localisation within the cage sites of $[Ca_{24}Al_{28}O_{64}]^{4+}(4e^-)$ was predicted. This led Medvedeva *et al.* to conclude that the excess electrons are too delocalized for this material to be considered an electride.[125]

Li *et al.*[127] subsequently noted that the embedded cluster model used by Sushko *et al.*[123] and the LMTO method used by Medvedeva *et al.*[125,126] conflict. They pointed out that the embedded cluster model is only accurate for a dilute extra-electron limit, while the LMTO model is potentially over-simplified to the point where it cannot accurately describe electrides. Additionally, neither method optimized the geometry of the $[Ca_{24}Al_{28}O_{64}]^{4+}(4e^-)$

crystal, leaving distortions present in the structure due to the removed O^{2-} ions. Li *et al.* conducted their own pseudopotential/planewave calculations using the projector-augmented wave (PAW)[134,135] approach and the Perdew-Wang exchange-correlation functional.[136] Optimisation of both distorted and undistorted initial crystal geometries converged to the same structure, with all crystal cage sizes equivalent.[127] Using the electron localisation function (ELF),[137,138] the primary type of bonding in the crystal was found to be ionic in nature, consistent with the electride model. Moreover, as reproduced in Figure 3, ELF analysis was able to identify localized charge within each cage, confirming that this crystal is an electride. The ELF thus provides a convenient method to detect interstitial electrons.

In this work we introduce an alternative analysis method to ELF, the Localized-Orbital Locator (LOL).[139,140] Both ELF and LOL possess similar theoretical constructions. In ELF, the essential variable is the electron pair density, while LOL relies on the local kinetic-energy density. Consequently, LOL has a slighly simpler functional form and benefits from more reliable asymptotic behaviour for atoms and small molecules.[140] ELF and LOL plots are provided in Figures 1,3-10(f) and (g), respectively, for all of the electrides presented in this work. Generally, the ELF and LOL reveal essentially same information.

7 - Property: The electron-localisation function (ELF) or localized-orbital locator (LOL) can be used to identify localized, interstitial electrons.
Problem: Similar to NCI, it can be difficult to visually distinguish isosurfaces enclosing the localized electrons from the other features of the ELF or LOL.

Sushko *et al.* performed additional calculations on $[Ca_{24}Al_{28}O_{64}]^{4+}(4e^-)$ in 2006,[128] this time using periodic-boundary conditions. The electrons were treated using Bloch functions, involving a linear combination of localized, atom-centred Gaussian-type basis functions and effective core potentials; three sets of s and p functions were included inside the empty cages. This study was aimed at examining the changing electronic properties as either O^{2-} or H^- dopants were gradually removed from the cages, increasing the density of interstitial electrons. Both the B3LYP and LDA density functionals were considered, with the LDA

Figure 3: Computed properties of the $[Ca_{24}Al_{28}O_{64}]^{4+}(4e^-)$ electride: a) the unit-cell geometry with the six atoms surrounding the central cage highlighted (black=Ca, orange=O) ; b) the band structure; c) the procrystal density, showing a 0.005 au isosurface; d) the density of the 'electride' band ($-1 < E < 0$ eV), showing a 0.001 au isosurface; e) the reduced density gradient used in NCI, showing a 0.5 au isosurface; f) the ELF, showing a 0.2 au isosurface; g) the LOL, showing a 0.2 au isosurface. All 2D plots map onto the (101) plane. The calculations used B86bPBE-XDM[64–66] with plane-wave and density-expansion cut-offs of 100 and 1000 Ry, and a $4 \times 4 \times 4$ k-point mesh. The crystal structure was obtained from the work of Bartl and Scheller.[67,131]

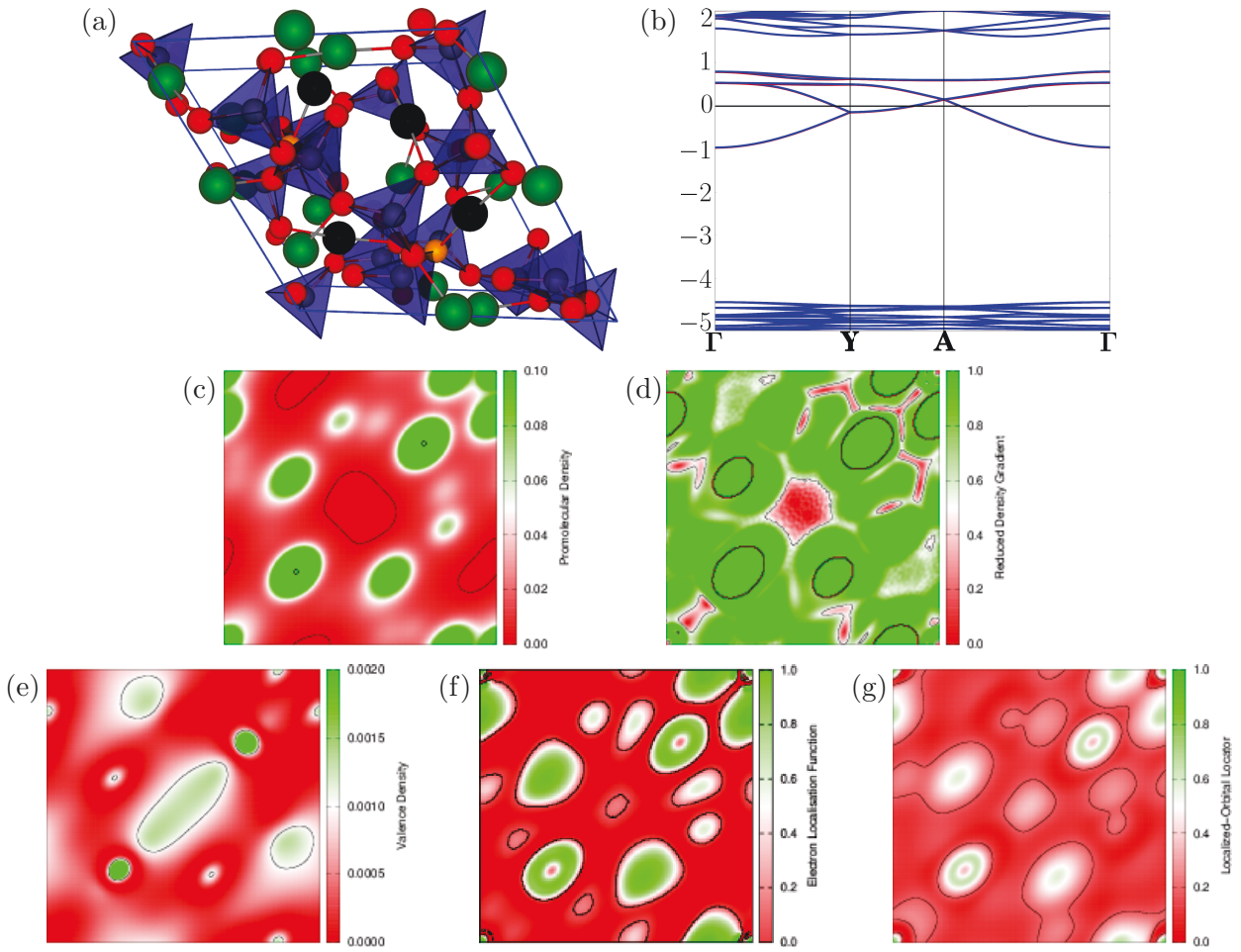

giving a consistently more delocalized picture of the interstitial electrons than B3LYP, as expected due to delocalisation error. The calculated band-gaps differed considerably, with the LDA indicating that $[Ca_{24}Al_{28}O_{64}]^{4+}(4e^-)$ becomes conducting even with very few interstitial electrons, while B3LYP always predicts the electride to be an insulator. It is worth

noting that, at higher density, both methods predict every cage to contain localized electrons, which seems to be in contradiction with the embedded cluster model used previously by that same group.[123]

The most recent theoretical study of $[Ca_{24}Al_{28}O_{64}]^{4+}(4e^-)$ by the Sushko group, focused on the different forms of the inorganic electride, specifically the crystalline, molten, and amorphous phases.[129] This study conducted molecular-dynamics simulations for a single, replicated unit cell of the crystal. Trajectories were acquired using the PBE functional[65] with projector augmented wave (PAW) pseudopotentials;[134,141] additional single-point energy calculations were conducted using the HSE hybrid functional.[86] Significant deformations in the crystal structure of $[Ca_{24}Al_{28}O_{64}]^{4+}(4e^-)$ were observed, which served to localize electron pairs at two different crystallographic sites. A calculated UV spectrum showed two peaks at 3.2 eV and 4.0 eV, and these values roughly correspond to the energy differences between the bonding and anti-bonding orbitals for each set of localized electron pairs.

Our own study of $[Ca_{24}Al_{28}O_{64}]^{4+}(4e^-)$ closely matched the results of Li *et al.*[127] and established consistency between this first inorganic electride and most of the properties observed for the existing organic electrides.[44] The calculated band structure of $[Ca_{24}Al_{28}O_{64}]^{4+}(4e^-)$ revealed an electride state (Property 2) with a much larger energy variation than seen for the organic electrides; this band structure is reproduced in Figure 3(b). The lack of band gap is consistent with the observed metallic conductivity, although the separation between the electride state and the lower-energy valence bands, is slightly underestimated.[121] Valence-density and NCI plots in Figure 3(e) and 3(c), respectively, reveal localized electron density in all 12 crystal cages (Properties 2 and 4). However, QTAIM analysis was unable to find NNMs (Property 3) in this case. It was speculated that this was due to both the smaller interstitial cages (relative to the organic electrides) and the shared/delocalized nature of the electride electrons in this particular material.[44]

Finally, Palacios *et al.*[130] conducted very high quality X-ray diffraction studies on the electride precursor, with 3 different levels of electron doping: $[Ca_{24}Al_{28}O_{64}]^{4+}O_{2-\delta}e^-_{2\delta}$ ($\delta =$

$0, 0.15, 0.45$), obtained by partial replacement of O^{2-} anions with localized electrons. For the $[Ca_{24}Al_{28}O_{64}]^{4+}O_{1.55}e^{-}_{0.9}$ electride, a localized electron density peak was detected,[130] but a similar feature has not been identified for the more concentrated iteration of this electride, $[Ca_{24}Al_{28}O_{64}]^{4+}(4e^{-})$. To date there has been no theoretical prediction of non-nuclear maxima in the electron density of $[Ca_{24}Al_{28}O_{64}]^{4+}(4e^{-})$, only electron localisation.

3.2 Elemental, extreme-pressure electrides

In 1997, high-pressure studies of sodium predicted the presence of a possible ionic state at pressures over 100 GPa.[142] A subsequent DFT study reinforced this prediction, specifically noting an "increasing valence electron density in the interstitial regions."[32] These predictions were later revealed to be correct, with the experimental observation of a metal-insulator transition during compression of sodium metal, subject to pressures over 200 GPa.[33] While the X-ray crystallography data acquired was insufficient to generate an exact crystal structure, one was predicted from first principles, using DFT and an evolutionary structure-generation methodology.[33] The resulting Na-hP4 structure, shown in Figure 4, was found to closely match the existing X-ray and Raman spectroscopy data. Subsequent band structure calculations and ELF analysis revealed a well-defined electride state, with a localized interstitial electron.[33,143,144]

A reproduction of the band structure and ELF for $Na^{+}e^{-}$ are provided in Figure 4(b) and (f), respectively. Note that the B86bPBE band structure does not show a well isolated electride state, in contrast to the original GW band structure calculation provided in the work of Ma *et al.*[33] The difference is due to the choice of density functional; generalised gradient approximation (GGA) functionals, such as B86bPBE, are known to significantly underestimate band gaps,[82–85] while the GW-DFT approximation partially corrects for this error.[145–147] This is an example of the type of errors that can occur in DFT studies of electrides and may explain why many of the inorganic electrides were predicted to be overly metallic based on PBE calculations.[11,36,37]

Figure 4: Computed properties of the Na^+e^- high-pressure electride: a) the unit-cell geometry; b) the band structure; c) the procrystal density, showing a 0.02 au isosurface; d) the density of the 'electride' band ($-1 < E < 0$ eV), showing a 0.005 au isosurface; e) the reduced density gradient used in NCI, showing a 0.5 au isosurface; f) the ELF, showing a 0.5 au isosurface; g) the LOL, showing a 0.5 au isosurface. All 2D plots map onto the (110) plane. The calculations used B86bPBE-XDM[64–66] with plane-wave and density-expansion cut-offs of 100 and 1000 Ry, and a $20 \times 20 \times 20$ k-point mesh. The crystal structure was reconstructed from information provided by Ma *et al.*[33]

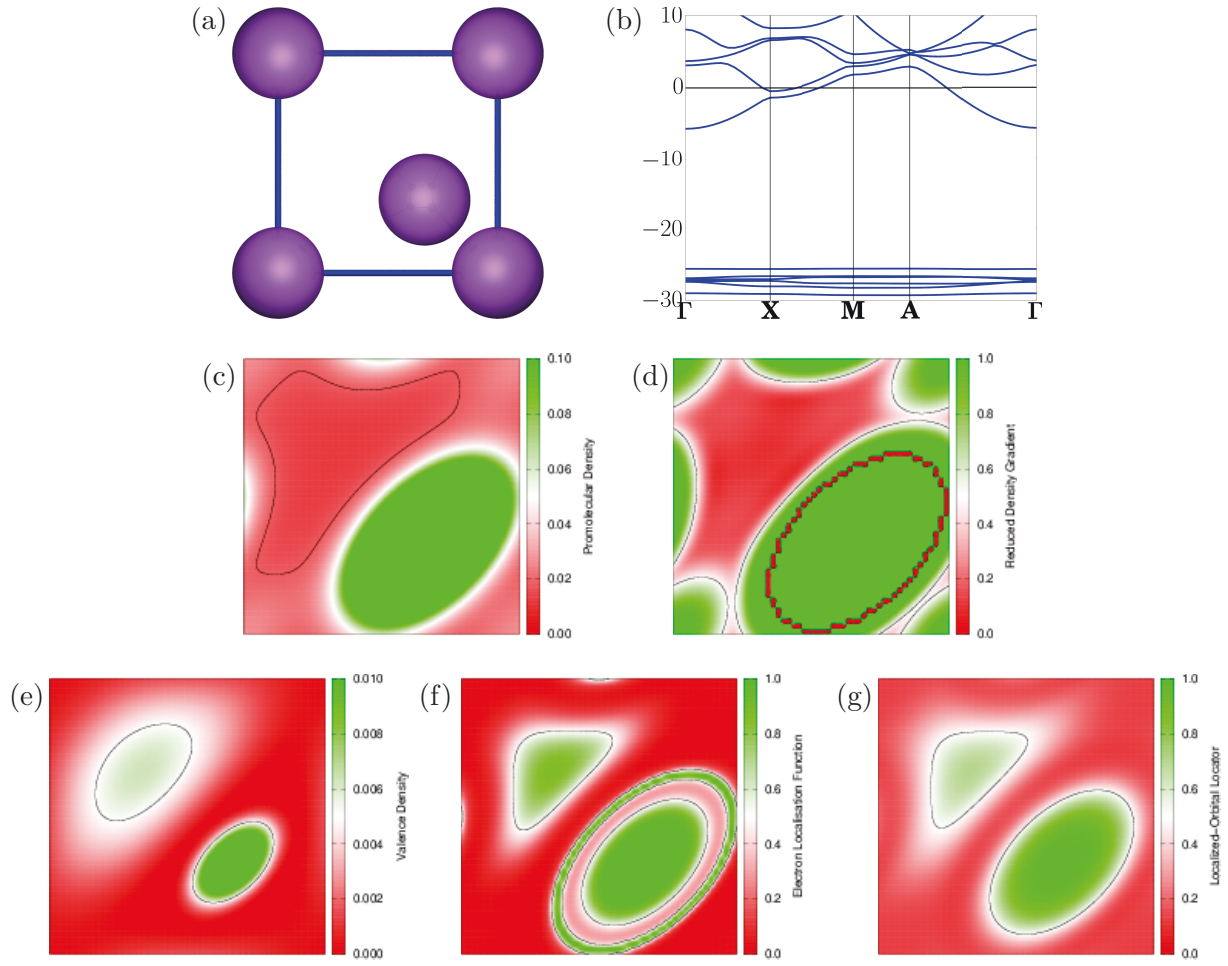

Similar electride states for other elemental materials have been theoretically predicted for a huge range of pressures using various evolutionary structure prediction techniques, but have yet to be experimentally confirmed. These elements include Li,[148–152] K,[153] Cs,[154,155] Mg,[156] Al,[156] and C,[157] at pressures ranging from 65 GPa to 30,000 GPa. $[Na_2He]^+e^-$, while not elemental, is also predicted to exist in an electride phase above 113 GPa.[158] Indeed, a model by Vegas *et al.*, which uses the electronic structure of the component metallic

matrix to interpret chemical bonding in crystalline solids, predicts that any metal lattice will express localized interstitial electron density at sufficiently high pressure.[159] Also, for the case of metallic Beryllium, there is evidence for non-nuclear maxima in the experimental electron-density distribution without any applied pressure.[160]

In 2014, Miao and Hoffman proposed that the localized electron in the high-pressure electrides behaves similarly to an atom and termed it an "interstitial quasi-atom" (ISQ).[161] It was argued that the energy levels of the ISQ increase in energy more slowly with applied pressure than do the energy levels of neighbouring valence orbitals. Thus, the ISQ will eventually become the minimum-energy state and the material will spontaneously form an electride at sufficiently high pressure. From studies of a simple model system under applied pressure, three general trends were found: (i) lowering the IP of the material makes it easier for an ISQ to form, (ii) decreasing the compressibility makes it easier for an ISQ to form, and (iii) occupied d-orbitals make it very hard for an ISQ to form. These trends, despite being strictly applicable only to elemental materials, appear consistent with some of the predictions for the organic electrides. Specifically, the requirement of a low IP matches with Property 6 for the IP of the alkali metal-ligand complexes that form the organic electrides. Additionally, the incompressibility of the atomic cores could be compared to the restrictive presence of the ligand molecules, effectively considering the alkali complexes as large, incompressible species in the solid crystal. Miao and Hoffman went on to demonstrate that the ISQs in elemental electride species can form pseudo-bonding and anti-bonding orbitals with neighbouring ISQs, leading to "quasi-molecules".[162,163]

3.3 2D electrides

In 2013, $[Ca_2N]^+e^-$ was identified as the first two-dimensional electride,[14] although the excess electron nature of this material was previously noted by Gregory *et al.*[164] $[Ca_2N]^+e^-$ is constructed of positively-charged, few-atom-thick layers, separated by regions of interstitial electron density. The atomic structure of the crystal is shown in Figure 5. The

relative simplicity of the unit cell of $[Ca_2N]^+e^-$ suggested that similar materials could also be electrides. Consequently, DFT calculations, evolutionary searches, and database screening methods, have been used to search for new 2D electrides, as was done for the elemental electrides.[165–173] The most successful of these studies searched through compounds in the MatNavi[174] and inorganic crystal structure database (ICSD)[175] and identified six potential 2D electrides. One of these materials, $[Y_2C]^{2+}2e^-$,[176,177] was experimentally characterised as an electride through photoelectron[39] and angle-resolved photoemission[178] spectroscopy. This was the second demonstration in the field that directed theoretical studies can guide experimental progress. Additionally, experimental measurements of $[Y_2C]^{2+}(2e^-)$ revealed anisotropic electronic and magnetic behaviour.[179]

Despite their recent discovery, a number of technological applications of 2D electrides have already been suggested. Both existing 2D electrides have been proposed as potential candidates for effective Na-ion battery anodes.[180,181] Additionally, interfacing an electride with another 2D material could serve as a means to modify that material's electronic properties.[182] $[Ca_2N]^+e^-$ was also shown to be a selective catalyst for hydrodehalgenation reactions and it was suggested that it could be similarly effective for other single-electron transfer reactions.[183] Finally, the unique optical properties of $[Ca_2N]^+e^-$, such as a negative refractive index, and the tunability of these properties under strain, have made this electride a new candidate for photonic device applications.[184,185]

DFT calculations on both $[Ca_2N]^+e^-$ and $[Y_2C]^{2+}(2e^-)$ reveal band structures with well localized electride states; the corresponding localized valence densities, ELF, LOL, and NCI plots reveal the interstitial electrons (plotted for $[Ca_2N]^+e^-$ in Figure 5(b)-(g)).[14,186,187] DFT also predicts that the magnetic properties of $[Y_2C]^{2+}(2e^-)$ originate from the localized anionic electrons (consistent with Property 5) and may exhibit itinerant ferromagnetic behaviour.[179] Further theoretical work suggests that the magnetic behaviour of $[Y_2C]^{2+}(2e^-)$ can be strategically modified through the application of pressure or appropriate doping,[188] and that high applied pressures will induce quenching of the material's electride properties.[189] Theoretical

Figure 5: Computed properties of the $[Ca_2N]^+e^-$ electride: a) the unit-cell geometry; b) the band structure; c) the procrystal density, showing a 0.01 au isosurface; d) the density of the 'electride' band ($-1 < E < 0$ eV), showing a 0.002 au isosurface; e) the reduced density gradient used in NCI, showing a 0.5 au isosurface; f) the ELF, showing a 0.5 au isosurface; g) the LOL, showing a 0.5 au isosurface. All 2D plots map onto the (011) plane. The calculations used B86bPBE-XDM[64–66] with plane-wave and density-expansion cut-offs of 100 and 1000 Ry, and a $12 \times 12 \times 1$ k-point mesh. The crystal structure was obtained from the work of Gregory *et al.*[67,164]

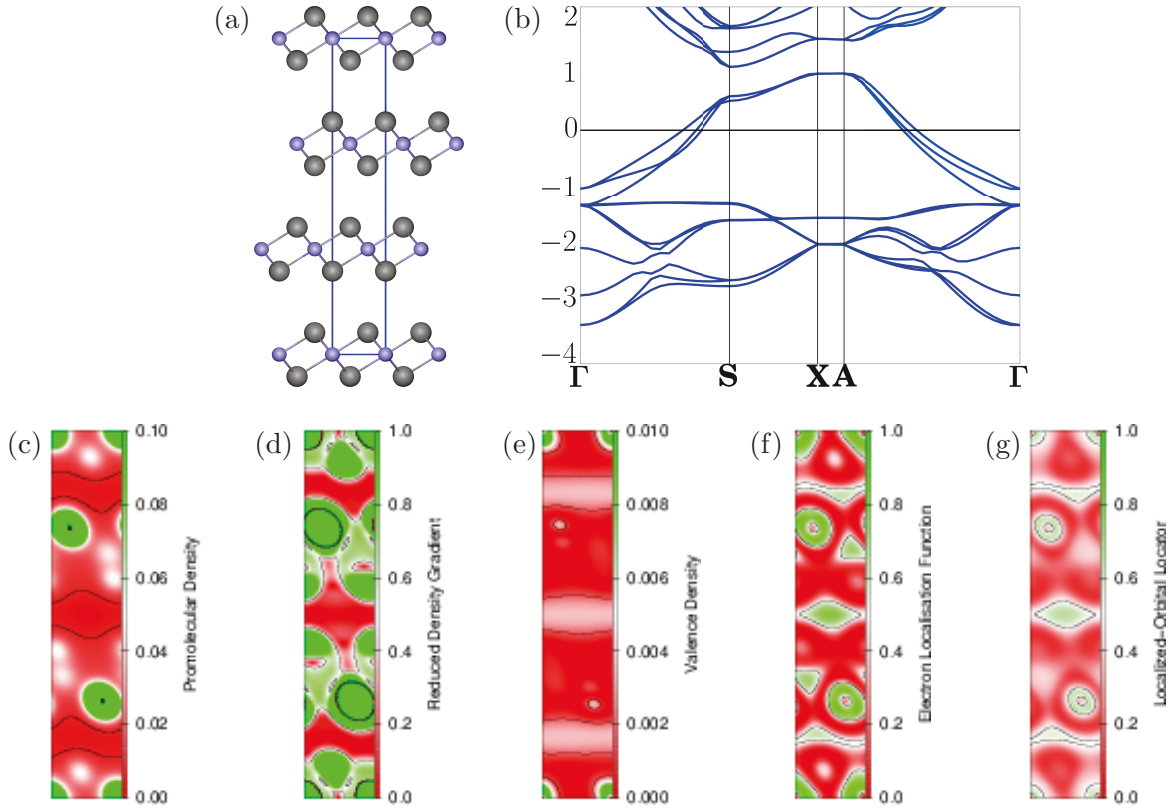

studies have also predicted that $[Y_2C]^{2+}(2e^-)$ is a low temperature superconductor[190,191] and a topological material.[192]

Exfoliation of single layers of $[Ca_2N]^+e^-$ from the bulk material was experimentally demonstrated, in 2016, by Druffel *et al.*[193] DFT calculations performed on single, exfoliated layers of both 2D electrides suggest that the excess electrons, no longer confined between the atomic layers, instead exist at the surface of these layers as a 2D pseudo free-electron gas.[187,194–196] Computational studies also predicted exfoliation of single layers to be feasi-

ble,[186,193,194] in advance of the experiments. However, the exfoliation energy is much larger than for typical 2D materials, such as graphite, hexagonal boron nitride, and molybdenum disulpide, consistent with the ionic nature of the electrides.[187] Conversely, interlayer sliding barriers for the 2D electrides were predicted to be extremely small, equivalent to typical 2D materials,[186,187] consistent with the expanded-metal nature of the electrides.[21]

3.4 Other inorganic electrides

After the initial discovery of $[Ca_{24}Al_{28}O_{64}]^{4+}(4e^-)$, almost all subsequent discoveries of inorganic electrides have been accompanied by DFT calculations of the band structure, density of states, electron density, and ELF. From 2015 to the present, 8 new inorganic electrides have been discovered. However, it is worth noting that the crystal structure of each new experimentally verifiable inorganic electride was previously known,[197–200] although the electride nature of these crystals generally went unidentified. This has led to the discovery of a number of electrides by scanning of crystallographic structural databases.[34,38,171] Many of these inorganic electrides have been found to be effective catalysts for N_2 splitting.[11,35,37,201]

$[La_8Sr_2(SiO_4)_6]^{4+}(4e^-)$ was discovered in 2015[34] by using DFT calculations to identify potential electride properties of known materials. This electride is both air and tempertature stable. It possesses a well defined electride state and localized electron in the ELF, LOL, NCI, and valence-density plots, as shown in Figure 6.

The lathanide hydrides of the form $[LnH_2]^+e^-$ (Ln = La, Ce or Y)), were also recently found to exhibit electride properties.[35] These are the first electrides to possess additional, formally anionic species, namely the hydride ions. DFT calculations were conducted on $[LaH_2]^+e^-$ and predicted an electride state in the band structure.[35] The band structure, valence density, NCI, ELF, and LOL are plotted in Figure 7. In this case the valence density does not reveal an obvious electride state. We also note that less accurate calculations, namely lower energy and density cut-offs and a smaller k-point mesh, obscure the localized electron identified by the ELF and LOL plots. This illustrates the sensitivity of predicted

Figure 6: Computed properties of the $[La_8Sr_2(SiO_4)_6]^{4+}(4e^-)$ electride: a) the unit-cell geometry; b) the band structure; c) the procrystal density, showing a 0.01 au isosurface; d) the density of the 'electride' band ($-1 < E < 0$ eV), showing a 0.005 au isosurface; e) the reduced density gradient used in NCI, showing a 0.5 au isosurface; f) the ELF, showing a 0.5 au isosurface; g) the LOL, showing a 0.5 au isosurface. All 2D plots map onto the (110) plane. The calculations used B86bPBE-XDM[64–66] with plane-wave and density-expansion cut-offs of 100 and 1000 Ry, and a $4\times4\times4$ k-point mesh. The crystal structure was obtained from the work of Sansom *et al.*[67,197]

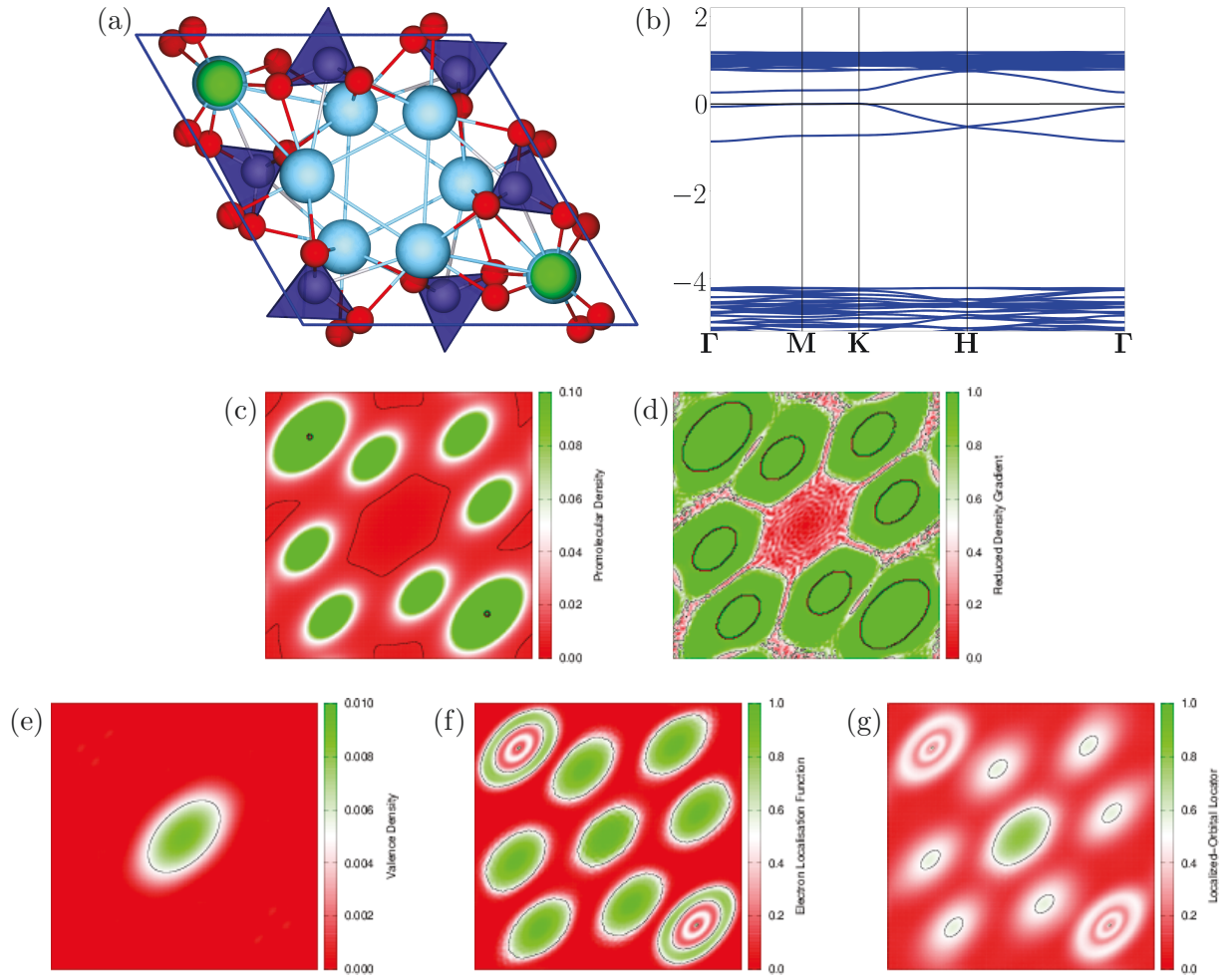

electride properties to the choice of DFT treatment.

Continuing the lathanide-based electride discoveries, $[La_2Sc_2Si_2]^3 3e^-$ was highlighted in 2017.[37] DFT calculations reveal an electride band that is not well isolated from the other electronic bands,[37] as shown in Figure 8. Because the 'electride' band cannot be isolated, the valence density is delocalized over a number of atoms and bonds, although there is still a distinct region of valence density within the central void. The valence density was

Figure 7: Computed properties of the $[LaH_2]^+e^-$ electride: a) the unit-cell geometry; b) the band structure; c) the procrystal density, showing a 0.01 au isosurface; d) the density of the 'electride' band ($-1 < E < 0$ eV), showing a 0.004 au isosurface; e) the reduced density gradient used in NCI, showing a 0.5 au isosurface; f) the ELF, showing a 0.5 au isosurface; g) the LOL, showing a 0.5 au isosurface. All 2D plots map onto the (110) plane. The calculations used B86bPBE-XDM[64–66] with plane-wave and density-expansion cut-offs of 100 and 1000 Ry, and a $12\times12\times12$ k-point mesh. The crystal structure was reconstructed from information provided in Mizoguchi *et al.*[35]

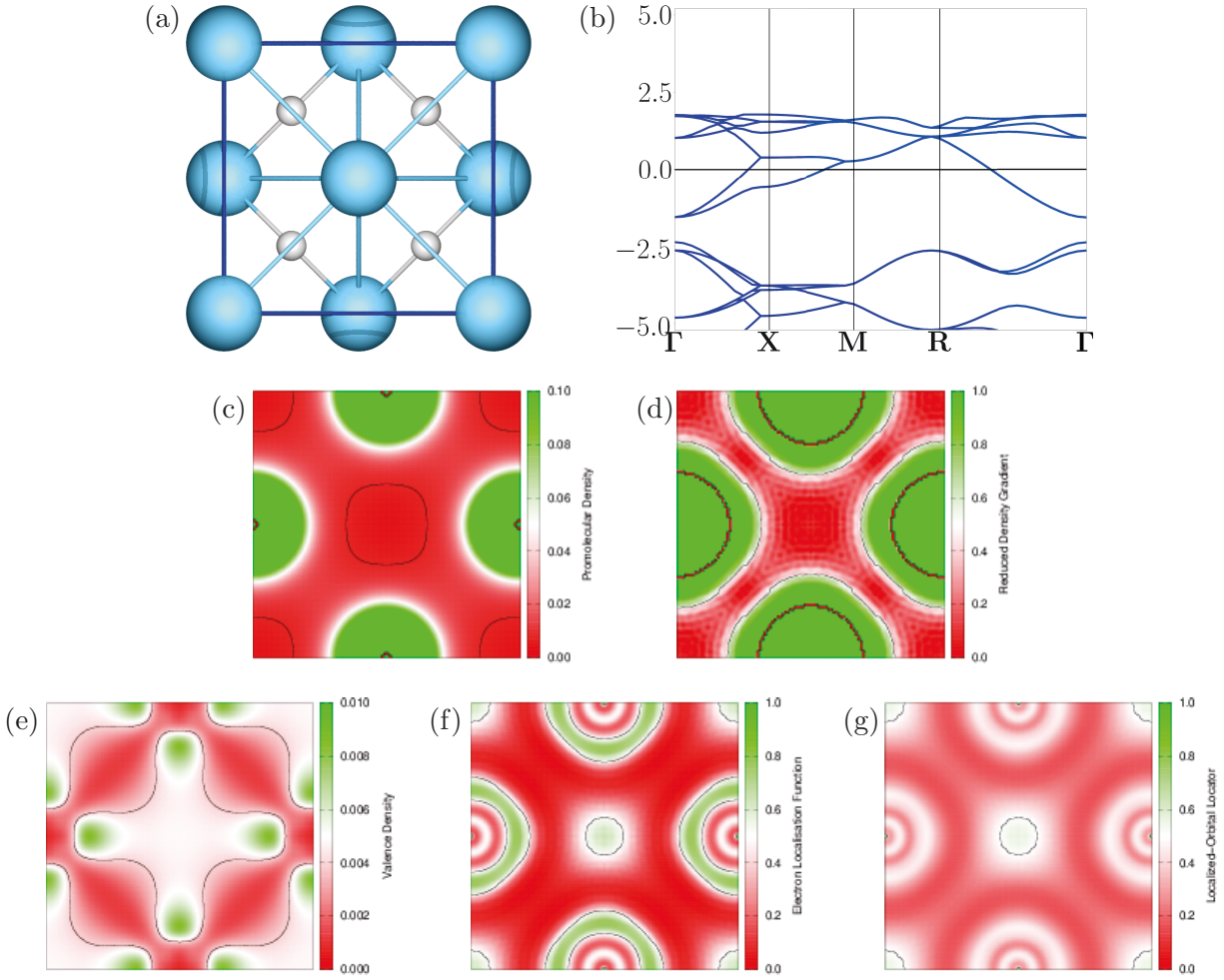

previously described as showing two distinct sites of electron localisation, and this material was coined a 'tiered' electride as a consequence.[37] We note that this tiered electron hierarchy is not a ground-state phenomenon, rather it appears as the electride is excited or doped with H atoms.[37] Both the promolecular density and NCI plots in Figure 8(c-d) show these two possible void sites, but the ELF and LOL plots in Figure 8(f-g) only show localized electrons at the single, central site. Indeed, $[La_2Sc_2Si_2]^3 3e^-$ is not the first electride to show a tiered

Figure 8: Computed properties of the $[La_2Sc_2Si_2]^3 3e^-$ electride: a) the unit-cell geometry; b) the band structure; c) the procrystal density, showing a 0.015 au isosurface; d) the density of the 'electride' band ($-0.1 < E < 0$ eV), showing a 0.0006 au isosurface; e) the reduced density gradient used in NCI, showing a 0.2 au isosurface; f) the ELF, showing a 0.5 au isosurface; g) the LOL, showing a 0.5 au isosurface. All 2D plots map onto the (101) plane. The calculations used B86bPBE-XDM[64–66] with plane-wave and density-expansion cut-offs of 100 and 1000 Ry, and a $6 \times 6 \times 6$ k-point mesh. The crystal structure was obtained from the work of Chevalier *et al.*[67,198]

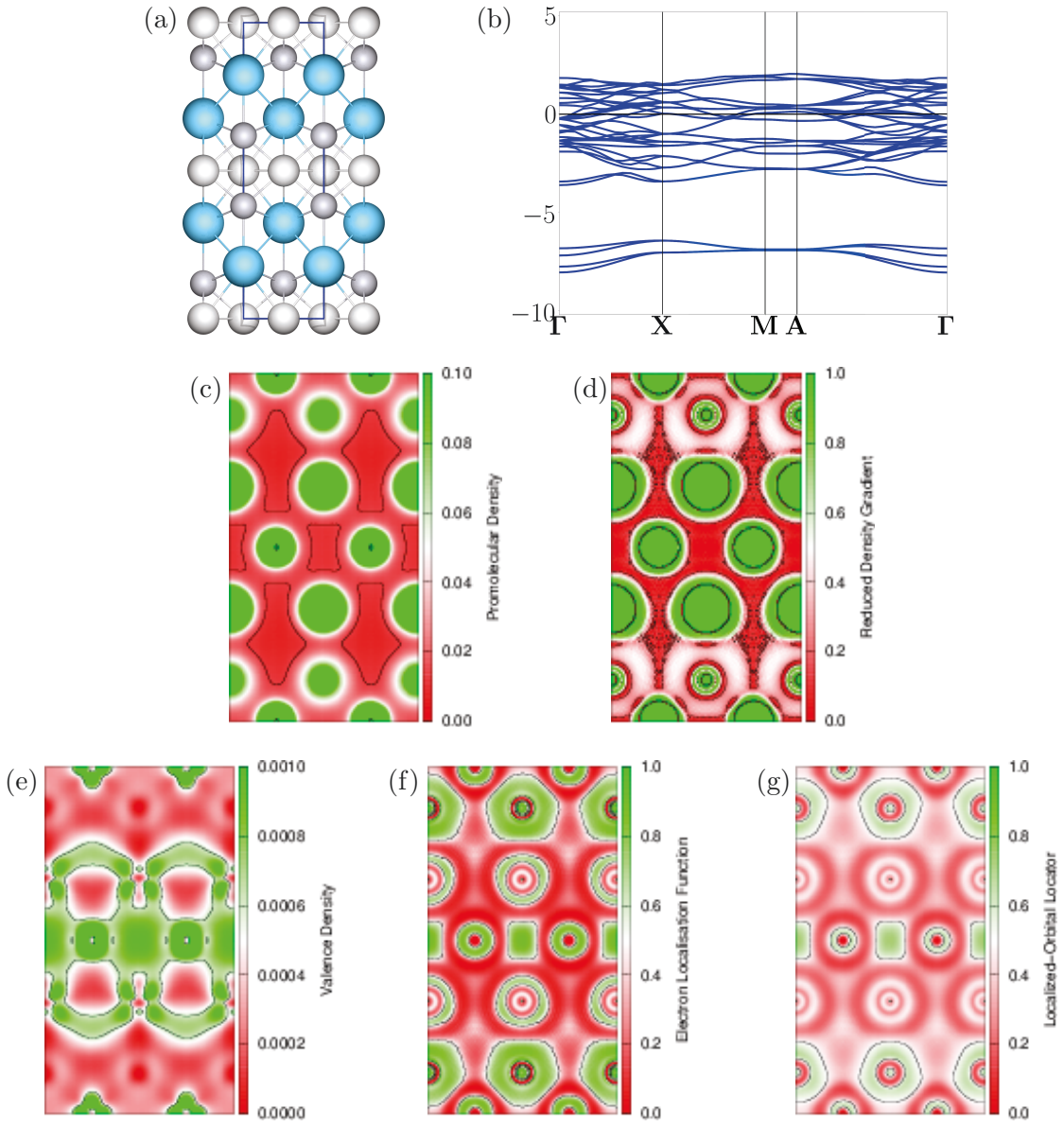

electron structure, as $[Cs^+(15C5)(18C6)e^-]_6(18C6)$ also possesses two distinct void sites, the smaller of which contains the lowest energy conduction band, while the larger contains the

electride band.[44,110]

Figure 9: Computed properties of the $[Y_5Si_3]^+e^-$ electride: a) the unit-cell geometry; b) the band structure; c) the procrystal density, showing a 0.012 au isosurface; d) the density of the 'electride' band ($-1 < E < 0$ eV), showing a 0.005 au isosurface; e) the reduced density gradient used in NCI, showing a 0.2 au isosurface; f) the ELF, showing a 0.5 au isosurface; g) the LOL, showing a 0.5 au isosurface. All 2D plots map onto the (110) plane. The calculations used B86bPBE-XDM[64–66] with plane-wave and density-expansion cut-offs of 100 and 1000 Ry, and a $8 \times 8 \times 8$ k-point mesh. The crystal structure was obtained from the work of Parthe.[67,199]

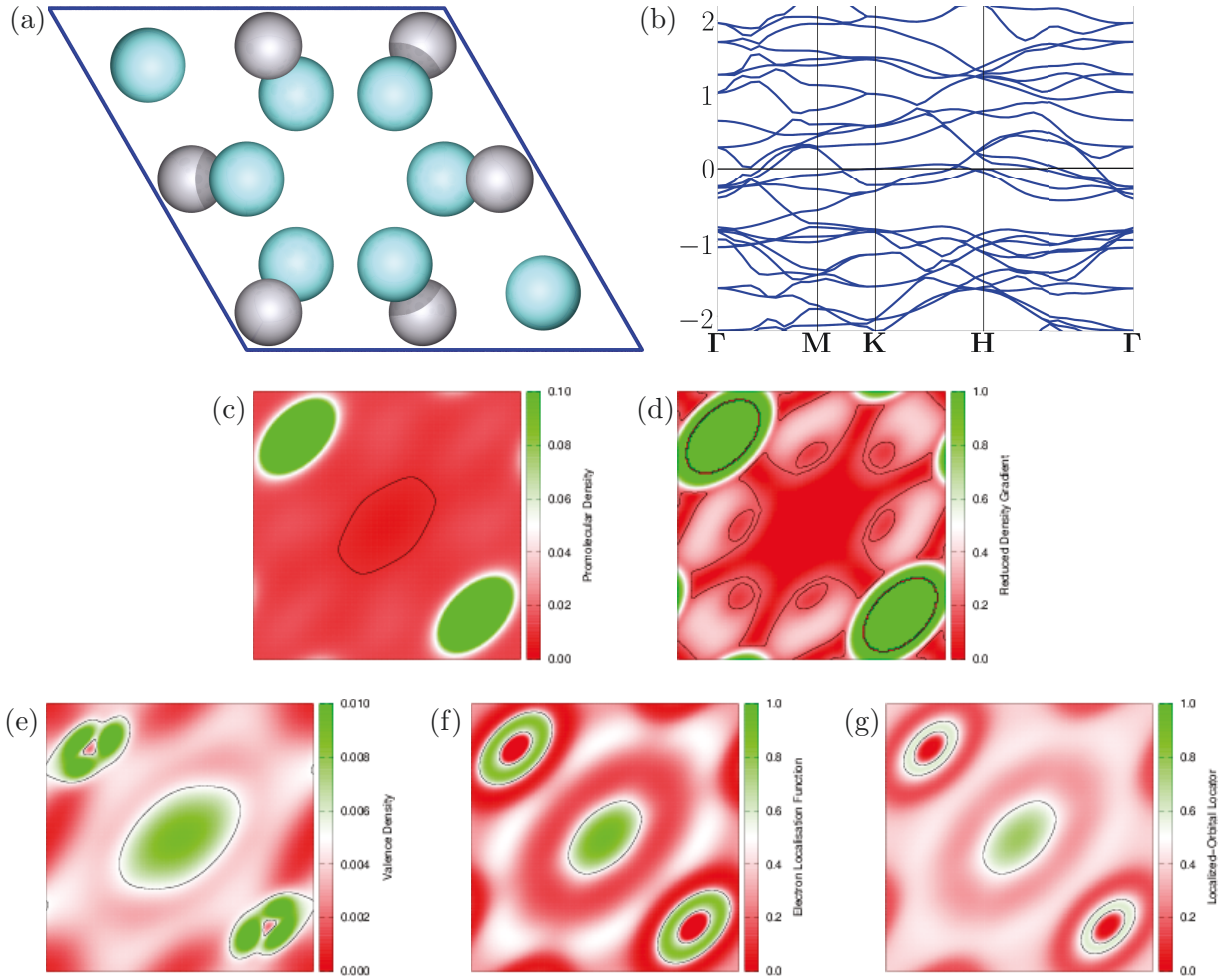

In 2016, $[Y_5Si_3]^+e^-$ was identified as the first temperature, atmosphere, and water stable electride,[11] which represented a significant advancement in the field. While an electride state exists for this material, it is not as well isolated in the band structure as for the electrides discussed previously. However, the ELF and LOL plots in Figure 9 clearly reveal a localized, interstitial electron.

Two other electrides that are isostructural to $[Y_5Si_3]^+e^-$ were also identified via DFT calculations. The first of these is $[Nb_5Ir_3]^{2+}(2e^-)$,[36] which is the only other electride to date (in addition to $[Ca_{24}Al_{28}O_{64}]^{4+}(4e^-)$) to exhibit a superconducting transition at ~ 3 K.[36] The DFT calculations[36] revealed very similar band structure and ELF plots to those obtained for $[Y_5Si_3]^+e^-$. The second such isostructural electride is $[Sr_5P_3]^+e^-$, which was identified via an *ab initio* evolutionary algorithm used to search for new electrides of composition Sr_xP_x.[38] By DFT screening of the generated structures, two new electrides were proposed (Sr_5P_3 and Sr_8P_5) and $[Sr_5P_3]^+e^-$ was subsequently experimentally verified.[38] The band structure of $[Sr_5P_3]^+e^-$ was found to reveal an electride state, the ELF showed a localized electron, and QTAIM analysis identifed a NNM, making it the only inorganic electride to possess one.[38] However, this previous work deliberately placed pseudo atoms at the intersitital sites and, if this is not done, NNM are not seen.

The Hosono group, which has discovered all of the inorganic electrides to date, typically uses the valence density for their identification.[14,34–36] However, for many of the inorganic electrides, particularly $[La_2Sc_2Si_2]^33e^-$, $[Y_5Si_3]^+e^-$, and $[Nb_5Ir_3]^{2+}e^{2-}$, the electride band is increasingly indistinct and cannot be isolated from the other valence and conduction bands, making the existence of such an 'electride' state a poor identifier of this class of electrides. As previously noted, LDA and GGA calculations are known to underestimate band gaps[82–85] and the overlap of the electride state with other bands may be a symptom of this. More accurate variants of DFT, such as hybrid functionals or the GW approximation, can correct this band gap underestimation.[145–147] While these methods come with a significant increase in computational cost and, consequently, can only be applied to simple unit cells, they could potentially be applied to this series of isostructural compounds to determine if electride states can indeed be isolated. Regardless of the convoluted band structure, the valence density continues to display a maximum in the interstitial regions, although it is partly delocalized over the adjacent atoms due to our inability to isolate the electride state.

4 Molecular electrides

The molecular electrides (sometimes called superalkalies) are a class of compounds that have been proposed and subsequently explored using theoretical models.[202–223] The first comparison of a molecular species to an electride was made by Chen *et al.*, in 2004, while investigating the water trimer anion.[203] Specifically, the observation was made that certain trimer configurations would form a strong dipole and the excess electron would occupy an extremely diffuse molecular orbital, localized at one end of the cluster. Note that these diffuse orbitals are very similar to the Rydberg-like states observed by Rencsok *et al.* in theoretical studies of the $Li^+(9C3)_2e^-$ complex.[57] Further, those configurations of the anionic water trimer possess exceptionally large hyperpolarisabilities. This can be justified as the hyperpolarisability is proportional to the difference in the dipole moment between the ground electronic state of the molecule and the relevant excited state.[205]

An exceptionally high hyperpolarisability is a particularly desirable property, essential to the function of non-linear optical (NLO) devices. This prompted the design of an 'electride molecule' to maximise the hyperpolarisability, by constructing or geometrically arranging complexants to 'push' or 'pull' the excess electron density from an alkali-metal atom to the extremes of the molecular system. In 2005, Chen *et al.*[204] designed the first such molecular electride, Li@Calix[4]pyrrole, the structure of which is given in Figure 10. Calix[4]pyrrole is a cone-like ligand with nitrogen atoms that coordinate to the Li atom, but repel the valence electron in a highly directional manner. This compound showed an extremely diffuse HOMO and large hyperpolarisability. In 2006, Chen *et al.* further showed that adding another alkali metal atom to Li@Calix[4]pyrrole, near the centre of the HOMO, would cause this alkali metal atom to bind the excess electron and form an alkalide-like compound, Li^+(Calix[4]pyrrole)M^-. This new 'molecular alkalide' retained the same exceptional hyperpolarisable properties as the molecular electrides.

An enormous number of molecular electrides have since been proposed using theoretical methods.[202–223] To give the reader a sense of scale, the highest measured hyperpolarisability

Figure 10: Computed properties of the Li@Calix[4]pyrrole molecular electride: a) the geometry; b) the band structure; c) the promolecular density, showing a 0.001 au isosurface; d) the density of the 'electride band' ($-1 < E < 0$ eV), showing a 0.001 au isosurface; e) the reduced density gradient used in NCI, showing a 0.5 au isosurface; f) the ELF, showing a 0.5 au isosurface; g) the LOL, showing a 0.5 au isosurface. All plots represent the vertical plane through the centre of the molecule. The calculations used B86bPBE-XDM[64–66] with plane-wave and density-expansion cut-off of 80 and 800 Ry, a $1 \times 1 \times 1$, inside a $20 \times 20 \times 20$ Å super-cell; atomic positions were previously relaxed in molecular calculations using B3LYP/6-31+G*.

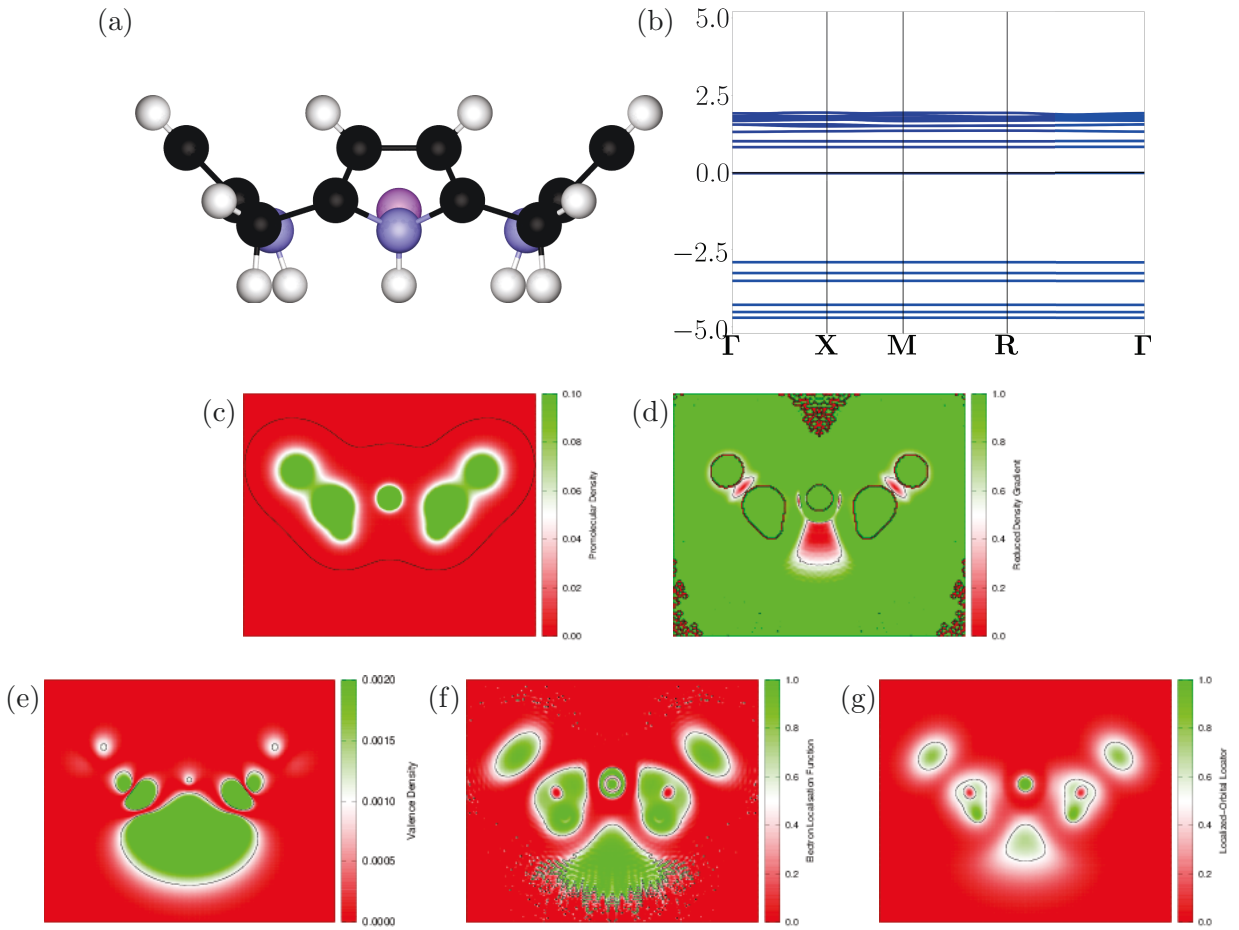

of a single molecule is 1.7×10^5 a.u.[224] In contrast, the calculated hyperpolarisiablilties of the molecular electrides have been reported to be as high as 1.7×10^7 a.u.,[203] and are regularly in excess of 1×10^5 a.u. Additionally, recent work has suggested that molecular electrides might contribute to the design of new anode materials for Li-based batteries.[223] However, while the theoretical results are clearly impressive, they must be treated with skepticism as

there is no experimental evidence to confirm or refute the existence of these materials, or to verify their predicted properties.

8 - Property: Electrides possess large non-linear optical properties.

Problem: This property may only be applicable to the molecular, rather than solid-state, electrides. Also, systems with such properties are not necessarily electrides.

In terms of their characterisation via DFT methods, Postils *et al.*,[219] concluded that the molecular electrides typically exhibit: (i) NNMs in the electron density, (ii) ELF basins for the excess electron, and (iii) large non-linear optical properties. The first two of these points have been identified in previous work on the organic or inorganic electrides, and are highlighted in this work as Properties 3 and 7, respectively. Large non-linear optical properties represent a new electride descriptor, although it is not clear to what extent this will be transferable to solid-state electrides. However, non-linear optical properties in the form of a tunable surface plasmon for a $[Ca_2N]^+e^-$ monolayer have been calculated.[185]

5 Summary

We have identified 8 properties, all based on electronic-structure theory predictions, that have been used to determine electride character within a material. However, as the various electride classes can have very different structural features, many of these properties are not generally transferable to all electrides. Further, a number of these properties are observable in materials that are not electrides (for example crystal voids are quite common in porous materials, such as metal-organic frameworks). Consequently, we wish to emphasise that the most reliable way to identify an electride is to establish that a given material reliably displays a number of these properties.

Special emphasis is placed on the void, band, NCI, ELF, and LOL properties, which are highlighted for selected electrides in Figures 1,3-10. The figures all include the computed electride band structures. Also shown are 2D contour plots of:

Table 1: Summary of properties used to identify electrides. (✓) implies this property is reliably observed. (✗) implies this property is not observed. (∼) implies this property is sometimes observed. (–) implies there is not enough information to make an informed judgement.

	1 (void)	2 (band)	3 (NNM)	4 (NCI)	5 (v-mag)	6 (thermo)	7 (ELF/LOL)	8 (NLO)
Org	✓	✓	✓	✓	✓	✓	✓	–
Inorg	✓	∼	✗	∼	∼	✗	✓	∼
Elem	✓	✓	✗	✓	–	∼	✓	–
2D	✓	✓	✗	∼	✓	✗	✓	∼
Molec	✗	∼	✓	✓	–	✓	✓	✓

1. the promolecular density, to allow visualisation of the crystal voids,

2. valence density corresponding to the electride band,

3. the reduced density gradient, used in NCI plots,

4. the electron localisation function, and

5. the localized-orbital locator.

All of the 2D plots generally depict the localized electron, at low isosurface values for the promolecular density and reduced density gradient, and at high isosurface values for the valence density, the ELF, and the LOL. Table 1 summarises which properties can be readily applied to identify electrides in each category.

The first property, the existence of crystal voids, has many obvious exceptions for common porous materials. Also, it is necessarily only applicable to the solid-state, and not to the molecular electrides. This same limitation applies to the existence of magnetic properties originating from unpaired, interstitial electrons (Property 5), with the added restriction that the elemental electrides and many of the inorganic electrides are not magnetic. Conversely, non-linear optical properties (8) are well established for the molecular electrides, but little is known regarding the transferability of this property to other electride classes. Only $[Ca_{24}Al_{28}O_{64}]^{4+}(4e^-)$, which has been used in fluorescent lighting, and $[Ca_2N]^+e^-$, for

which plasmon calculations have been conducted,[185] have established optical properties. The thermochemical requirement of strong cation-ligand binding and a low ionization potential (Property 6) is primarily limited to the organic and molecular electrides, although the low-IP requirement is also relevant to elemental electrides. The existence of NNMs is a good descriptor of organic and molecular electrides. However, the more compact nature of the voids in the inorganic and elemental electrides precludes the detection of NNMs, despite the accumulation of density in the interstitial regions. Also, NNMs are common in many simple molecules, such as Li_2 and C_2H_2, which are not electrides. Thus, the identification of crystal voids, non-nuclear density maxima, and magnetic, thermodynamic, or non-linear optical properties, are all only applicable to particular classes of electride materials. None of these properties are sufficiently general to be unambiguous descriptors of electrides.

The presence of high-energy valence bands, with densities residing within the voids (Property 2), is an excellent descriptor to identify solid-state electrides, as illustrated in Figures 1,3-6. While this property is also limited to solid-state electrides in its strictest interpretation, the molecular electrides do have a high-energy HOMO, similar to that of a Rydberg state, that localizes on one end of the molecule, as shown in Figure 10. However, the band structures can become quite complex for inorganic electrides, making it extremely difficult to identify for which band the valence density should be plotted.

This leaves the other density-based properties, specifically the existence of basins in either the reduced density gradient (NCI, Property 4), or in the electron localisation function and localized-orbital locator (ELF and LOL, Property 7), as the most general descriptors of electrides. NCI can be viewed as a generalisation of the NNM property, relaxing the requirement of zero gradient to also include regions of low reduced density gradients. As shown in Figures 1,3-10, this criteria seems to allow detection of all electride classes. However, this NCI analysis is dependent on the ability of the user to distinguish the appearance of localized, interstitial electrons from the various other types of non-covalent or bonding interactions that typically appear these plots.

The ELF and LOL appear to be the most reliable tools for the identification of electride behaviour. While the same danger of misidentification highlighted for NCI is still possible, the information delivered by these methods is much simpler to interpret, and this danger is mitigated. To avoid this danger completely, we recommend using multiple electride identification properties concurrently. Consequently, we find that ELF and LOL plots are the best descriptors of the properties considered for general identification of electrides.

Finally, the majority of the tools suggested in this work to identify an electride material rely on theoretical calculations employing density-functional approximations. It is therefore important to recognise that errors in these methods can bias the assessments made. If an insufficiently accurate electronic-structure calculation is performed, the density will be inadequate for identification of electrides, no matter how well suited the chosen screening method is to this task. The most prominent existing error in density-functional approximations is delocalisation error (also known as self-interaction error and charge-transfer error).[68–79] Studies have been conducted to assess the impact of delocalisation error when investigating electride materials and, as the name suggests, found the density distribution of the 'localized' electron to be excessively diffuse.[75,80,81] Therefore, the rule of thumb is that electrides are more likely to go unidentified due to inherent errors in the modelling methods. The present work highlighted a few potential examples of this. Notably, $[LaH_2]^+e^-$ and $[La_2Sc_2Si_2]^3(3e^-)$ failed to be identified as electrides by all density assessment methods if the energy and density cut-off values and k-point mesh were only slightly lower than those used in Figures 7 and 8. Moreover, the electride band of Na^+e^- was difficult to identify when using a pure GGA functional, while the application of GW-DFT made the electride band easily identifiable. We postulate that a similar improvement in theoretical treatment could also better isolate the electride bands in $[Y_5Si_3]^+e^-$ and its related, isostructural electrides.

In summary, it is quickly becoming apparent that the electride phenomena is not rare, but is simply difficult to identify. This difficulty manifests in both experimental and theoretical techniques, which have served to develop the field in tandem. As the electride materials

are explored further, we are gaining a deeper understanding of unusual chemical bonding situations and access to a host of new materials. While a number of potential applications for these materials have been explored, more complex control and utilisation of their unique electronic structure remains as open field. The future of electride research is laced with potential.

6 Acknowledgements

The authors would like to acknowledge Dr. Alberto Otero-de-la-Roza for helpful discussions and technical support when using the critic2 program. S. G. D would like to acknowledge Prof. Axel D. Becke for ongoing support and insightful discussions. We also thank the Natural Sciences and Engineering Research Council of Canada (NSERC) for financial support.

References

(1) Dye, J. L. Electrides: Early Examples of Quantum Confinement. *Acc. Chem. Res.* **2009**, *42*, 1564.

(2) Buchammagari, H.; Toda, Y.; Hirano, M.; Hosono, H.; Takeuchi, D.; Osakada, K. Room temperature-stable electride as a synthetic organic reagent: application to pinacol coupling reaction in aqueous media. *Org. Lett.* **2007**, *9*, 4287.

(3) Choi, S.; Kim, Y. J.; Kim, S. M.; Yang, J. W.; Kim, S. W.; Cho, E. J. Hydrotrifluoromethylation and iodotrifluoromethylation of alkenes and alkynes using an inorganic electride as a radical generator. *Nat. Commun.* **2014**, *5*, 4881.

(4) Kim, Y. J.; Kim, S. M.; Hosono, H.; Yang, J. W.; Kim, S. W. The scalable pinacol coupling reaction utilizing the inorganic electride $[Ca_2N]^+ \cdot e^-$ as an electron donor. *Chem. Comm.* **2014**, *50*, 4791.

(5) Kim, Y. J.; Kim, S. M.; Cho, E. J.; Hosono, H.; Yang, J. W.; Kim, S. W. Two dimensional inorganic electride-promoted electron transfer efficiency in transfer hydrogenation of alkynes and alkenes. *Chem. Sci.* **2015**, *6*, 3577.

(6) Yanagi, H.; Kim, K.-B.; Koizumi, I.; Kikuchi, M.; Hiramatsu, H.; Miyakawa, M.; Kamiya, T.; Hirano, M.; Hosono, H. Low Threshold Voltage and Carrier Injection Properties of Inverted Organic Light-Emitting Diodes with $[Ca_{24}Al_{28}O_{64}]^{4+}(4e^{-})$ Cathode and $Cu_{2-x}Se$ Anode. *J. Phys. Chem. C* **2009**, *113*, 18379.

(7) Li, J.; Yin, B.; Fuchigami, T.; Inagi, S.; Hosono, H.; Ito, S. Application of $12CaO{\cdot}7Al_2O_3$ electride as a new electrode for superoxide ion generation and hydroxylation of an arylboronic acid. *Electrochem. Commun.* **2012**, *17*, 52.

(8) Toda, Y.; Hirayama, H.; Kuganathan, N.; Torrisi, A.; Sushko, P. V.; Hosono, H. Activation and splitting of carbon dioxide on the surface of an inorganic electride material. *Nat. Commun.* **2013**, *4*, –.

(9) Kitano, M.; Inoue, Y.; Yamazaki, Y.; Hayashi, F.; Kanbara, S.; Matsuishi, S.; Yokoyama, T.; Kim, S.-W.; Hara, M.; Hosono, H. Ammonia synthesis using a stable electride as an electron donor and reversible hydrogen store. *Nat. Chem.* **2012**, *4*, 934.

(10) Kitano, M.; Kanbara, S.; Inoue, Y.; Kuganathan, N.; Sushko, P. V.; Yokoyama, T.; Hara, M.; Hosono, H. Electride support boosts nitrogen dissociation over ruthenium catalyst and shifts the bottleneck in ammonia synthesis. *Nat. Commum.* **2015**, *6*, –.

(11) Lu, Y.; Li, J.; Tada, T.; Toda, Y.; Ueda, S.; Yokoyama, T.; Kitano, M.; Hosono, H. Water Durable Electride Y_5Si_3: Electronic Structure and Catalytic Activity for Ammonia Synthesis. *J. Am. Chem. Soc.* **2016**, *138*, 3970.

(12) Watanabe, S.; Watanabe, T.; Ito, K.; Miyakawa, N.; Ito, S.; Hosono, H.; Mikoshiba, S.

Secondary electron emission and glow discharge properties of $12CaO{\cdot}7Al_2O_3$ electride for fluorescent lamp applications. *Sci. Technol. Adv. Mat.* **2011**, *12*, 034410.

(13) Miyakawa, M.; Kim, S. W.; Hirano, M.; Kohama, Y.; Kawaji, H.; Atake, T.; Ikegami, H.; Kono, K.; Hosono, H. Superconductivity in an Inorganic Electride $12CaO{\cdot}7Al_2O_3{:}e^-$. *J. Am. Chem. Soc.* **2007**, *129*, 7270.

(14) Lee, K.; Kim, S. W.; Toda, Y.; Matsuishi, S.; Hosono, H. Dicalcium nitride as a two-dimensional electride with an anionic electron layer. *Nature* **2013**, *494*, 336.

(15) Edwards, P. P. From solvated elecvtrons to metal anions: Electronic-structure and dynamics. *J. Solution Chem.* **1985**, *14*, 187.

(16) Kraus, C. A. Solutions of metals in non-metallic solvents; I. general properties of solutions of metals in liquid ammonia. *J. Am. Chem. Soc.* **1907**, *29*, 1557.

(17) Pedersen, C. J. Cyclic polyethers and their complexes with metal salts. *J. Am. Chem. Soc.* **1967**, *89*, 7017.

(18) Lehn, J. M. *Alkali Metal Complexes with Organic Ligands*; 1973; pp 1–69.

(19) Tehan, F. J.; Barnett, B. L.; Dye, J. L. Alkali anions. Preparation and crystal structure of a compound which contains the cryptated sodium cation and the sodium anion. *J. Am. Chem. Soc.* **1974**, *96*, 7203.

(20) Dye, J. L.; Ceraso, J. M.; Lok, M.; Barnett, B.; Tehan, F. J. Crystalline salt of the sodium anion (Na-). *J. Am. Chem. Soc.* **1974**, *96*, 608.

(21) Wagner, M. J.; Dye, J. L. Alkalides, Electrides and Expanded Metals. *Annu. Rev. Mater.* **1994**, *25*, 223.

(22) Ellaboudy, A.; Dye, J. L.; Smith, P. B. Cesium 18-crown-6 compounds. A crystalline ceside and a crystalline electride. *J. Am. Chem. Soc.* **1983**, *105*, 6490.

(23) Dawes, S. B.; Ward, D. L.; Huang, R. H.; Dye, J. L. First electride crystal structure. *J. Am. Chem. Soc.* **1986**, *108*, 3534.

(24) Ward, D. L.; Huang, R.; Dye, J. L. Structures of alkalides and electrides. I. Structure of potassium cryptand [2.2.2] electride. *Acta Crystallogr. C* **1988**, *44*, 1374.

(25) Ward, D.; Huang, R.; Dye, J. The structures of alkalides and electrides. III. Structure of potassium cryptand [2.2.2] natride. *Acta Crystallogr C* **1990**, *46*, 1833.

(26) Ward, D. L.; Huang, R.; Dye, J. L. The structures of alkalides and electrides. V. Structures of caesium bis (15-crown-5) kalide and rubidium bis (15-crown-5) rubidide. *Acta Crystallogr C* **1990**, *46*, 1838.

(27) Wagner, M. J.; Huang, R. H.; Eglin, J. L.; Dye, J. L. An electride with a large six-electron ring. *Nature* **1994**, *368*, 726.

(28) Huang, R. H.; Wagner, M. J.; Gilbert, D. J.; Reidy-Cedergren, K. A.; Ward, D. L.; Faber, M. K.; Dye, J. L. Structure and Properties of Li^+(cryptand [2.1.1])e^-, an Electride with a 1D Spin-Ladder-like Cavity-Channel Geometry. *J Am. Chem. Soc.* **1997**, *119*, 3765.

(29) Xie, Q.; Huang, R. H.; Ichimura, A. S.; Phillips, R. C.; Pratt, W. P.; Dye, J. L. Structure and Properties of a New Electride, Rb^+(cryptand[2.2.2])e^-. *J. Am. Chem. Soc.* **2000**, *122*, 6971.

(30) Redko, M. Y.; Jackson, J. E.; Huang, R. H.; Dye, J. L. Design and Synthesis of a Thermally Stable Organic Electride. *J. Am. Chem. Soc.* **2005**, *127*, 12416.

(31) Matsuishi, S.; Toda, Y.; Miyakawa, M.; Hayashi, K.; Kamiya, T.; Hirano, M.; Tanaka, I.; Hosono, H. High-density electron anions in a nanoporous single crystal: $[Ca_{24}Al_{28}O_{64}]^{4+}(4e^-)$. *Science* **2003**, *301*, 626.

(32) Neaton, J. B.; Ashcroft, N. W. On the constitution of sodium at higher densities. *Phys. Rev. Lett.* **2001**, *86*, 2830.

(33) Ma, Y.; Eremets, M.; Oganov, A. R.; Xie, Y.; Trojan, I.; Medvedev, S.; Lyakhov, A. O.; Valle, M.; Prakapenka, V. Transparent dense sodium. *Nature* **2009**, *458*, 182.

(34) Zhang, Y.; Xiao, Z.; Kamiya, T.; Hosono, H. Electron Confinement in Channel Spaces for One-Dimensional Electride. *J. Phys. Chem. Lett.* **2015**, *6*, 4966.

(35) Mizoguchi, H.; Okunaka, M.; Kitano, M.; Matsuishi, S.; Yokoyama, T.; Hosono, H. Hydride-Based Electride Material, LnH_2 (Ln= La, Ce, or Y). *Inorg. Chem.* **2016**, *55*, 8833.

(36) Zhang, Y.; Wang, B.; Xiao, Z.; Lu, Y.; Kamiya, T.; Uwatoko, Y.; Kageyama, H.; Hosono, H. Electride and superconductivity behaviors in Mn_5Si_3-type intermetallics. *npj Quantum Materials* **2017**, *2*, 45.

(37) Wu, J.; Gong, Y.; Inoshita, T.; Fredrickson, D. C.; Wang, J.; Lu, Y.; Kitano, M.; Hosono, H. Tiered electron anions in multiple voids of LaScSi and their applications to ammonia synthesis. *Adv. Mater.* **2017**, *29*.

(38) Wang, J.; Hanzawa, K.; Hiramatsu, H.; Kim, J.; Umezawa, N.; Iwanaka, K.; Tada, T.; Hosono, H. Exploration of Stable Strontium Phosphide-Based Electrides: Theoretical Structure Prediction and Experimental Validation. *J. Am. Chem. Soc.* **2017**, *139*, 15668.

(39) Zhang, X.; Xiao, Z.; Lei, H.; Toda, Y.; Matsuishi, S.; Kamiya, T.; Ueda, S.; Hosono, H. Two-Dimensional Transition-Metal Electride Y_2C. *Chem. Mater.* **2014**, *26*, 6638.

(40) Huang, R.; Faber, M.; Moeggenborg, K.; Ward, D.; Dye, J. Structure of K^+(cryptand [2.2.2]) electride and evidence for trapped electron pairs. *Nature* **1988**, *331*, 599.

(41) Dawes, S. B.; Eglin, J. L.; Moeggenborg, K. J.; Kim, J.; Dye, J. L. $Cs^+(15\text{-crown-}5)_2e^-$. A crystalline antiferromagnetic electride. *J. Am. Chem. Soc.* **1991**, *113*, 1605.

(42) Ichimura, A. S.; Wagner, M. J.; Dye, J. L. Anisotropic Charge Transport and Spin-Spin Interactions in K^+(cryptand [2.2.2]) Electride. *J. Phys. Chem. B* **2002**, *106*, 11196.

(43) Dye, J. L.; Wagner, M. J.; Overney, G.; Huang, R. H.; Nagy, T. F.; Tomanek, D. Cavities and channels in electrides. *J. Am. Chem. Soc.* **1996**, *118*, 7329.

(44) Dale, S. G.; Otero-de-la Roza, A.; Johnson, E. R. Density-functional description of electrides. *Phys. Chem. Chem. Phys.* **2014**, *16*, 14584.

(45) Spackman, M. A.; Maslen, E. N. Chemical properties from the promolecule. *J. Phys. Chem.* **1986**, *90*, 2020.

(46) Turner, M. J.; McKinnon, J. J.; Jayatilaka, D.; Spackman, M. A. Visualisation and characterisation of voids in crystalline materials. *Cryst. Eng. Comm.* **2011**, *13*, 1804.

(47) Dawes, S. B.; Ellaboudy, A. S.; Dye, J. L. Cesium-133 solid-state nuclear magnetic resonance spectroscopy of alkalides and electrides. *J. Am. Chem. Soc.* **1987**, *109*, 3508.

(48) Beckmann, A.; Böklen, K.; Elke, D. Precision measurements of the nuclear magnetic dipole moments of 6 Li, 7 Li, 23 Na, 39 K and 41 K. *Z. Phys.* **1974**, *270*, 173–186.

(49) Dye, J. L.; Andrews, C. W.; Ceraso, J. M. Nuclear magnetic resonance studies of alkali metal anions. *J. Phys. Chem.* **1975**, *79*, 3076.

(50) Ellaboudy, A.; Tinkham, M. L.; Van Eck, B.; Dye, J. L.; Smith, P. B. Magic-angle spinning sodium-23 nuclear magnetic resonance studies of crystalline sodides. *J. Phys. Chem.* **1984**, *88*, 3852–3855.

(51) Tinkham, M. L.; Dye, J. L. First observation by potassium-39 NMR of K-in solution and in crystalline potassides. *J. Am. Chem. Soc.* **1985**, *107*, 6129.

(52) Edwards, P. P.; Ellaboudy, A. S.; Holton, D. M. NMR spectrum of the potassium anion K-. *Nature* **1985**, *317*, 242.

(53) Pyper, N.; Edwards, P. P. Nuclear shielding in the alkali metal anions. *J. Am. Chem. Soc.* **1986**, *108*, 78–81.

(54) Holton, D. M.; Edwards, P. P.; Johnson, D. C.; Page, C. J.; McFarlane, W.; Wood, B. Multielement NMR and ESR study of solutions of the alkali metals sodium to cesium in N,N-diethylacetamide, N,N-dipropylacetamide, N,N-dimethylpropanamide, and tetramethylurea. *J. Am. Chem. Soc.* **1985**, *107*, 6499–6504.

(55) Tinkham, M. L.; Ellaboudy, A.; Dye, J. L.; Smith, P. B. Detection of rubidide anion (Rb^-) in crystalline rubidides by rubidium-87 nuclear magnetic resonance. *J. Phys. Chem.* **1986**, *90*, 14–16.

(56) Golden, S.; Tuttle Jr, T. R. Spectral-moment constraints on electride-electron locations in the crystalline electride [Cs(18-crown-6)$_2$]. *Phys. Rev. B* **1992**, *45*, 13913.

(57) Rencsok, R.; Kaplan, T.; Harrison, J. On the electronic structure of electrides. *J. Chem. Phys.* **1990**, *93*, 5875.

(58) Kaplan, T.; Rencsok, R.; Harrison, J. Valence-electron distribution of cesium crown-ether electrides. *Phys. Rev. B* **1994**, *50*, 8054.

(59) Golden, S.; Tuttle Jr, T. R. Electride-electron locations in the crystalline electride [Cs(18-crown-6)$_2$]: Nonuniqueness of current quantum-mechanical models. *Phys. Rev. B* **1994**, *50*, 8059.

(60) Rencsok, R.; Kaplan, T. A.; Harrison, J. F. Electronic structure of Li(9-crown-3)$_2$: A molecule with a Rydberg-type ground state. *J. Chem. Phys.* **1993**, *98*, 9758.

(61) Allan, G.; De Backer, M.; Lannoo, M.; Lefebvre, I. Why Do the Electrons Play the Role of Anions in the Electrides? *Europhys. Lett.* **1990**, *11*, 49.

(62) Lefebvre, I.; Lannoo, M.; Allan, G.; Ibanez, A.; Fourcade, J.; Jumas, J. C.; Beaurepaire, E. Electronic Properties of Antimony Chalcogenides. *Phys. Rev. Lett.* **1987**, *59*, 2471.

(63) Singh, D.; Krakauer, H.; Haas, C.; Pickett, W. Theoretical determination that electrons act as anions in the electride $Cs^+(15\text{-crown-}5)_2e^-$. *Nature* **1993**, *365*, 39.

(64) Becke, A. On the large-gradient behavior of the density functional exchange energy. *J. Chem. Phys.* **1986**, *85*, 7184.

(65) Perdew, J.; Burke, K.; Ernzerhof, M. Generalized gradient approximation made simple. *Phys. Rev. Lett.* **1996**, *77*, 3865.

(66) Otero-de-la Roza, A.; Johnson, E. R. Van der Waals Interactions in Solids Using the Exchange-Hole Dipole Moment Model. *J. Chem. Phys.* **2012**, *136*, 174109.

(67) Allen, F. H. The Cambridge Structural Database: a quarter of a million crystal structures and rising. *Acta. Crystallogr. B* **2002**, *58*, 380.

(68) Ruiz, E.; Salahub, D. R.; Vela, A. Charge-transfer complexes: Stringent tests for widely used density functionals. *J. Phys. Chem.* **1996**, *100*, 12265.

(69) Ruzsinszky, A.; Perdew, J. P.; Csonka, G. I.; Vydrov, O. A.; Scuseria, G. E. Spurious fractional charge on dissociated atoms: Pervasive and resilient self-interaction error of common density functionals. *J. Chem. Phys.* **2006**, *125*, 194112.

(70) Ruzsinszky, A.; Perdew, J. P.; Csonka, G. I.; Vydrov, O. A.; Scuseria, G. E. Density functionals that are one- and two- are not always many-electron self-interaction-free, as shown for H_2^+, He_2^+, LiH^+, and Ne_2^+. *J. Chem. Phys.* **2007**, *126*, 104102.

(71) Cohen, A. J.; Mori-Sánchez, P.; Yang, W. Insights into current limitations of density functional theory. *Science* **2008**, *321*, 792–794.

(72) Heaton-Burgess, T.; Yang, W. Structural manifestation of the delocalization error of density functional approximations: C_{4N+2} rings and C_{20} bowl, cage, and ring isomers. *J. Chem. Phys.* **2010**, *132*, 234113.

(73) Steinmann, S. N.; Piemontesi, C.; Delacht, A.; Corminboeuf, C. Why are the Interaction Energies of Charge-Transfer Complexes Challenging for DFT? *J. Chem. Theory Comput.* **2012**, *8*, 1629.

(74) Johnson, E. R.; Salamone, M.; Bietti, M.; DiLabio, G. A. Modeling Noncovalent Radical-Molecule Interactions Using Conventional Density-Functional Theory: Beware Erroneous Charge Transfer. *J. Phys. Chem. A.* **2013**, *117*, 947.

(75) Johnson, E. R.; Otero-de-la Roza, A.; Dale, S. G. Extreme density-driven delocalization error for a model solvated-electron system. *J. Chem. Phys.* **2013**, *139*, 184116.

(76) Otero-de-la Roza, A.; Johnson, E. R.; DiLabio, G. A. Halogen bonding from dispersion-corrected density-functional theory: The role of delocalization error. *J. Chem. Theory Comput.* **2014**, *10*, 5436–5447.

(77) Kim, M.-C.; Sim, E.; Burke, K. Understanding and reducing errors in density functional calculations. *Phys. Rev. Lett.* **2013**, *111*, 073003.

(78) Kim, M.-C.; Sim, E.; Burke, K. Ions in solution: Density corrected density functional theory (DC-DFT). *J. Chem. Phys.* **2014**, *140*, 18A528.

(79) Kim, M.-C.; Park, H.; Son, S.; Sim, E.; Burke, K. Improved DFT potential energy surfaces via improved densities. *J. Phys. Chem. Lett.* **2015**, *6*, 3802–3807.

(80) Janesko, B. G.; Scalmani, G.; Frisch, M. J. Quantifying solvated electrons' delocalization. *Phys. Chem. Chem. Phys.* **2015**, *17*, 18305.

(81) Janesko, B. G.; Scalmani, G.; Frisch, M. J. Quantifying Electron Delocalization in Electrides. *J. Chem. Theor. Comput.* **2015**, *12*, 79.

(82) Seidl, A.; Görling, A.; Vogl, P.; Majewski, J.; Levy, M. Generalized Kohn-Sham schemes and the band-gap problem. *Phys. Rev. B* **1996**, *53*, 3764.

(83) Perdew, J. P.; Ruzsinszky, A.; Constantin, L. A.; Sun, J.; Csonka, G. I. Some Fundamental Issues in Ground-State Density Functional Theory: A Guide for the Perplexed. *J. Chem. Theory Comput.* **2009**, *5*, 902.

(84) Becke, A. D. Perspective: Fifty years of density-functional theory in chemical physics. *J. Chem. Phys.* **2014**, *140*, 18A301.

(85) Pribram-Jones, A.; Gross, D. A.; Burke, K. DFT: A theory full of holes? *Ann. Rev. Phys. Chem.* **2015**, *66*, 283–304.

(86) Krukau, A. V.; Vydrov, O. A.; Izmaylov, A. F.; Scuseria, G. E. Influence of the exchange screening parameter on the performance of screened hybrid functionals. *J. Chem. Phys.* **2006**, *125*, 224106.

(87) Becke, A. D. Density-functional thermochemistry. III. The role of exact exchange. *J. Chem. Phys.* **1993**, *98*, 5648.

(88) O'Reilly, E.; Robertson, J. Electronic structure of amorphous III-V and II-VI compound semiconductors and their defects. *Phys. Rev. B* **1986**, *34*, 8684.

(89) Zhukovskii, Y. F.; Kotomin, E. A.; Evarestov, R. A.; Ellis, D. E. Periodic models in quantum chemical simulations of F centers in crystalline metal oxide. *Int. J. Quantum Chem.* **2007**, *107*, 2956.

(90) Bader, R. F. *Atoms in molecules*; 1990.

(91) Bader, R. F. A quantum theory of molecular structure and its applications. *Chem. Rev.* **1991**, *91*, 893.

(92) Matta, C. F.; Boyd, R. J. *The quantum theory of atoms in molecules: from solid state to DNA and drug design*; 2007.

(93) Gatti, C. Chemical bonding in crystals: New directions. *Z. Kristallogr.* **2005**, *220*, 399.

(94) Johnson, E. R.; Keinan, S.; Mori-Sánchez, P.; Contreras-García, J.; Cohen, A. J.; Yang, W. Revealing Noncovalent Interactions. *J. Am. Chem. Soc.* **2010**, *132*, 6498.

(95) Otero-de-la Roza, A.; Johnson, E. R.; Contreras-García, J. Revealing non-covalent interactions in solids: NCI plots revisited. *Phys. Chem. Chem. Phys.* **2012**, *14*, 12165.

(96) Otero-de-la-Roza, A.; Johnson, E. R.; Luãna, V. Critic2: A program for real-space analysis of quantum chemical interactions in solids. *Comput. Phys. Commun.* **2014**, *185*, 1007.

(97) Yu, M.; Trinkle, D. R. Accurate and efficient algorithm for Bader charge integration. *J. Chem. Phys.* **2011**, *134*, 064111.

(98) Otero-de-la Roza, A.; Johnson, E. R.; Luaña, V. Critic2: a program for real-space analysis of quantum chemical interactions in solids. *Comp. Phys. Comm.* **2014**, 1007.

(99) Bader, R.; Platts, J. Characterization of an F-center in an alkali halide cluster. *The J. Chem. Phys.* **1997**, *107*, 8545.

(100) Madsen, G.; Gatti, C.; Iversen, B.; Damjanovic, L.; Stucky, G.; Srdanov, V. F center in sodium electrosodalite as a physical manifestation of a non-nuclear attractor in the electron density. *Phys. Rev. B* **1999**, *59*, 12359.

(101) Mori-Sanchez, P.; Recio, J.; Silvi, B.; Sousa, C.; Pendás, A. M.; Luaña, V.; Illas, F. Rigorous characterization of oxygen vacancies in ionic oxides. *Phys. Rev. B* **2002**, *66*, 075103.

(102) Cioslowski, J. Nonnuclear attractors in the lithium dimeric molecule. *J. Phys. Chem.* **1990**, *94*, 5496.

(103) Pendás, A. M.; Blanco, M. A.; Costales, A.; Sánchez, P. M.; Luaña, V. Non-nuclear maxima of the electron density. *Phys. Rev. Lett.* **1999**, *83*, 1930.

(104) Dye, J. L. Electrides: From 1D Heisenberg Chains to 2D Pseudo-Metals. *Inorg. Chem.* **1997**, *36*, 3816.

(105) Wagner, M. J.; Ichimura, A. S.; Huang, R. H.; Phillips, R. C.; Dye, J. L. Cs^+(18-crown-6)$_2e^-$: A 1D Heisenberg Antiferromagnet with Unusual Phase Transitions. *J. Phys. Chem. B* **2000**, *104*, 1078.

(106) Ryabinkin, I. G.; Staroverov, V. N. Interelectron magnetic coupling in electrides with one-dimensional cavity-channel geometry. *Phys. Chem. Chem. Phys.* **2011**, *13*, 21615.

(107) Ryabinkin, I. G.; Staroverov, V. N. Solution of the Schrödinger equation for two electrons in axially symmetric cavities. *Phys. Rev. A* **2010**, *82*, 022505.

(108) Ryabinkin, I. G.; Staroverov, V. N. Two electrons in a cylindrical box: An exact configuration-interaction solution. *Phys. Rev. A* **2010**, *81*, 032509.

(109) Wagner, M.; Dye, J. [Cs^+(15-Crown-5)(18-Crown-6)e^-]$_6$·(18-Crown-6): Properties of the First Mixed Crown Ether Electride. *J. Solid State Chem.* **1995**, *117*, 309.

(110) Dale, S. G.; Johnson, E. R. The explicit examination of the magnetic states of electrides. *Phys. Chem. Chem. Phys.* **2016**, *18*, 27326.

(111) Kim, T. J.; Yoon, H.; Han, M. J. Calculating magnetic interactions in organic electrides. *Phys. Rev. B* **2018**, *97*, 214431.

(112) Dale, S. G.; Otero-de-la Roza, A.; Johnson, E. R. Pressure-Induced Isostructural Antiferromagnetic-Ferromagnetic Transition in an Organic Electride. *J. Phys. Chem. C* **2018**, *122*, 12742.

(113) Dale, S. G.; Johnson, E. R. Thermodynamic cycles of the alkali metal-ligand complexes central to electride formation. *Phys. Chem. Chem. Phys.* **2017**, *19*, 12819.

(114) Petkov, V.; Billinge, S. J. L.; Vogt, T.; Ichimura, A. S.; Dye, J. L. Structure of intercalated Cs in zeolite ITQ-4: An array of metal ions and correlated electrons confined in a pseudo-1D nanoporous host. *Phys. Rev. Lett.* **2002**, *89*, 075502.

(115) Ichimura, A. S.; Dye, J. L.; Camblor, M. A.; Villaescusa, L. A. Toward Inorganic Electrides. *J. Am. Chem. Soc.* **2002**, *124*, 1170.

(116) Li, Z.; Yang, J.; Hou, J. G.; Zhu, Q. Inorganic Electride: Theoretical Study on Structural and Electronic Properties. *J. Am. Chem. Soc.* **2003**, *125*, 6050.

(117) Dye, J. L. Electrons as Anions. *Science* **2003**, *301*, 607.

(118) Li, H.; Mahanti, S. D. Theoretical Study of Encapsulated Alkali Metal Atoms in Nanoporous Channels of ITQ-4 Zeolite: One-Dimensional Metals and Inorganic Electrides. *Phys. Rev. Lett.* **2004**, *93*, 216406.

(119) Kim, S. W.; Shimoyama, T.; Hosono, H. Solvated Electrons in High-Temperature Melts and Glasses of the Room-Temperature Stable Electride $[Ca_{24}Al_{28}O_{64}]^{4+}(4e^{-})$. *Science* **2011**, *333*, 71.

(120) Toda, Y.; Matsuishi, S.; Hayashi, K.; Ueda, K.; Kamiya, T.; Hirano, M.; Hosono, H. Field emission of electron anions clathrated in subnanometer-sized cages in $[Ca_{24}Al_{28}O_{64}]^{4+}(4e^{-})$. *Adv. Mater.* **2004**, *16*, 685.

(121) Toda, Y.; Yanagi, H.; Ikenaga, E.; Kim, J. J.; Kobata, M.; Ueda, S.; Kamiya, T.; Hirano, M.; Kobayashi, K.; Hosono, H. Work Function of a Room-Temperature, Stable Electride $[Ca_{24}Al_{28}O_{64}]^{4+}(4e^{-})$. *Adv. Mater.* **2007**, *19*, 3564.

(122) Kim, S. W.; Matsuishi, S.; Nomura, T.; Kubota, Y.; Takata, M.; Hayashi, K.; Kamiya, T.; Hirano, M.; Hosono, H. Metallic State in a Lime-Alumina Compound with Nanoporous Structure. *Nano Lett.* **2007**, *7*, 1138.

(123) Sushko, P. V.; Shluger, A. L.; Hayashi, K.; Hirano, M.; Hosono, H. Electron localization and a confined electron gas in nanoporous inorganic electrides. *Phys. Rev. Lett.* **2003**, *91*, 126401.

(124) Sushko, P. V.; Shluger, A. L.; Hayashi, K.; Hirano, M.; Hosono, H. Localisation assisted by the lattice relaxation and the optical absorption of extra-framework electrons in $12CaO{\cdot}7Al_2O_3$. *Mat. Sci. Eng. C* **2005**, *25*, 722.

(125) Medvedeva, J. E.; Freeman, A. J. Hopping versus bulk conductivity in transparent oxides: $12CaO{\cdot}7Al_2O_3$. *Appl. Phys. Lett.* **2004**, *85*, 955.

(126) Medvedeva, J. E.; Freeman, A. J.; Bertoni, M. I.; Mason, T. O. Electronic structure and light-induced conductivity of a transparent refractory oxide. *Phys. Rev. Lett.* **2004**, *93*, 016408.

(127) Li, Z.; Yang, J.; Hou, J.; Zhu, Q. Is mayenite without clathrated oxygen an inorganic electride? *Angew. Chem. Int. Edit.* **2004**, *43*, 6479.

(128) Sushko, P. V.; Shluger, A. L.; Hirano, M.; Hosono, H. From Insulator to Electride: A Theoretical Model of Nanoporous Oxide $12CaO{\cdot}7Al_2O_3$. *J. Am. Chem. Soc.* **2007**, *129*, 942.

(129) Johnson, L. E.; Sushko, P. V.; Tomota, Y.; Hosono, H. Electron anions and the glass transition temperature. *P. Natl. Acad. Sci. USA* **2016**, *113*, 10007.

(130) Palacios, L.; Cabeza, A.; Bruque, S.; García-Granda, S.; Aranda, M. A. Structure and electrons in mayenite electrides. *Inorg. Chem.* **2008**, *47*, 2661.

(131) Bartl, H.; Scheller, T. *Neues Jahrb. Mineral. Monatsh.* **1970**, *35*, 547.

(132) Zacate, M. O.; Grimes, R. W. Simulation of Al/Fe disorder in $Ca_2Fe_xAl_{2x}O_5$. *J. Phys. Chem. Solids* **2002**, *63*, 675.

(133) Keller, J. Modified muffin tin potentials for the band structure of semiconductors. *J. Phys. C.* **1971**, *4*, 85.

(134) Blöchl, P. E. Projector augmented-wave method. *Phys. Rev. B* **1994**, *50*, 17953.

(135) Kresse, G.; Furthmüller, J. Efficient iterative schemes for ab initio total-energy calculations using a plane-wave basis set. *Phys. Rev. B* **1996**, *54*, 11169.

(136) Perdew, J. P.; Chevary, J. A.; Vosko, S. H.; Jackson, K. A.; Pederson, M. R.; Singh, D. J.; Fiolhais, C. Atoms, molecules, solids, and surfaces: Applications of the generalized gradient approximation for exchange and correlation. *Phys. Rev. B* **1992**, *46*, 6671.

(137) Silvi, B.; Savin, A. Classification of chemical bonds based on topological analysis of electron localization functions. *Nature* **1994**, *371*, 683.

(138) Becke, A. D.; Edgecombe, K. E. A simple measure of electron localization in atomic and molecular systems. *J. Chem. Phys.* **1990**, *92*, 5397.

(139) Becke, A. D. Simulation of delocalized exchange by local density functionals. *J. Chem. Phys.* **2000**, *112*, 4020–4026.

(140) Schmider, H.; Becke, A. Chemical content of the kinetic energy density. *J. Mol. Struct. Theochem* **2000**, *527*, 51–61.

(141) Kresse, G.; Joubert, D. From ultrasoft pseudopotentials to the projector augmented-wave method. *Phys. Rev. B* **1999**, *59*, 1758.

(142) Siringo, F.; Pucci, R.; Angilella, G. G. Are light alkali metals still metals under high pressure? *High Pressure Res.* **1997**, *15*, 255.

(143) Gatti, M.; Tokatly, I. V.; Rubio, A. Sodium: a charge-transfer insulator at high pressures. *Phys. Rev. Lett.* **2010**, *104*, 216404.

(144) Marqués, M.; Santoro, M.; Guillaume, C. L.; Gorelli, F. A.; Contreras-García, J.; Howie, R. T.; Goncharov, A. F.; Gregoryanz, E. Optical and electronic properties of dense sodium. *Phys. Rev. B* **2011**, *83*, 184106.

(145) van Schilfgaarde, M.; Kotani, T.; Faleev, S. Quasiparticle Self-Consistent GW Theory. *Phys. Rev. Lett.* **2006**, *96*, 226402.

(146) Zanolli, Z.; Fuchs, F.; Furthmüller, J.; von Barth, U.; Bechstedt, F. Model GW band structure of InAs and GaAs in the wurtzite phase. *Phys. Rev. B* **2007**, *75*, 245121.

(147) Rinke, P.; Janotti, A.; Scheffler, M.; Van de Walle, C. G. Defect Formation Energies without the Band-Gap Problem: Combining Density-Functional Theory and the GW Approach for the Silicon Self-Interstitial. *Phys. Rev. Lett.* **2009**, *102*, 026402.

(148) Ma, Y.; Oganov, A. R.; Xie, Y. High-pressure structures of lithium, potassium, and rubidium predicted by an ab initio evolutionary algorithm. *Phys. Rev. B* **2008**, *78*, 014102.

(149) Pickard, C. J.; Needs, R. Dense low-coordination phases of lithium. *Phys. Rev. Lett.* **2009**, *102*, 146401.

(150) Yao, Y.; John, S. T.; Klug, D. D. Structures of insulating phases of dense lithium. *Phys. Rev. Lett.* **2009**, *102*, 115503.

(151) Lv, J.; Wang, Y.; Zhu, L.; Ma, Y. Predicted novel high-pressure phases of lithium. *Phys. Rev. Lett.* **2011**, *106*, 015503.

(152) Rousseau, B.; Xie, Y.; Ma, Y.; Bergara, A. Exotic high pressure behavior of light alkali metals, lithium and sodium. *Eur. Phys. J. B* **2011**, *81*, 1.

(153) Marqués, M.; Ackland, G. J.; Lundegaard, L. F.; Stinton, G.; Nelmes, R. J.; McMahon, M. I.; Contreras-García, J. Potassium under Pressure: A Pseudobinary Ionic Compound. *Phys. Rev. Lett.* **2009**, *103*, 115501.

(154) Takemura, K.; Christensen, N.; Novikov, D.; Syassen, K.; Schwarz, U.; Hanfland, M. Phase stability of highly compressed cesium. *Phys. Rev. B* **2000**, *61*, 14399.

(155) Zurek, E.; Jepsen, O.; Andersen, O. K. Muffin-Tin Orbital Wannier-Like Functions for Insulators and Metals. *ChemPhysChem* **2005**, *6*, 1934.

(156) Pickard, C. J.; Needs, R. Aluminium at terapascal pressures. *Nat. Mater.* **2010**, *9*, 624.

(157) Martinez-Canales, M.; Pickard, C. J.; Needs, R. J. Thermodynamically stable phases of carbon at multiterapascal pressures. *Phys. Rev. Lett.* **2012**, *108*, 045704.

(158) Dong, X. et al. A stable compound of helium and sodium at high pressure. *Nat. Chem.* **2017**, *9*, 440.

(159) Vegas, A.; Santamaría-Pérez, D.; Marqués, M.; Flórez, M.; Baonza, V. G.; Recio, J. M. Anions in metallic matrices model: application to the aluminium crystal chemistry. *Acta Cryst. B* **2006**, *62*, 220–227.

(160) Iversen, B. B.; Larsen, F. K.; Souhassou, M.; Takata, M. Experimental evidence for the existence of non-nuclear maxima in the electron-density distribution of metallic beryllium. A compartive study of the maximum entropy method and the multipole refinement method. *Acta Cryst. B* **1995**, *51*, 580–591.

(161) Miao, M.-S.; Hoffmann, R. High pressure electrides: a predictive chemical and physical theory. *Acc. Chem. Res.* **2014**, *47*, 1311.

(162) Miao, M.-S.; Hoffmann, R. High-Pressure Electrides: The Chemical Nature of Interstitial Quasiatoms. *J. Am. Chem. Soc.* **2015**, *137*, 3631.

(163) Miao, M.-s.; Hoffmann, R.; Botana, J.; Naumov, I. I.; Hemley, R. J. Quasimolecules in Compressed Lithium. *Angew. Chem. Int. Edit.* **2017**, *129*, 992.

(164) Gregory, D. H.; Bowman, A.; Baker, C. F.; Weston, D. P. Dicalcium nitride, $[Ca_2N]e^-$ 2D "excess electron" compound; synthetic routes and crystal chemistry. *J. Mater. Chem.* **2000**, *10*, 1635.

(165) Walsh, A.; Scanlon, D. O. Electron excess in alkaline earth sub-nitrides: 2D electron gas or 3D electride? *J. Mater. Chem. C* **2013**, *1*, 3525.

(166) Tada, T.; Takemoto, S.; Matsuishi, S.; Hosono, H. High-throughput ab initio screening for two-dimensional electride materials. *Inorg. Chem.* **2014**, *53*, 10347.

(167) Inoshita, T.; Jeong, S.; Hamada, N.; Hosono, H. Exploration for Two-Dimensional Electrides via Database Screening and Ab Initio Calculation. *Phys. Rev. X* **2014**, *4*, 031023.

(168) Zhang, Y.; Wang, H.; Wang, Y.; Zhang, L.; Ma, Y. Computer-Assisted Inverse Design of Inorganic Electrides. *Phys. Rev. X* **2017**, *7*, 011017.

(169) Tsuji, Y.; Dasari, P. L.; Elatresh, S.; Hoffmann, R.; Ashcroft, N. Structural Diversity and Electron Confinement in Li_4N: Potential for 0-D, 2-D, and 3-D Electrides. *J. Am. Chem. Soc.* **2016**, *138*, 14108.

(170) Ming, W.; Yoon, M.; Du, M.-H.; Lee, K.; Kim, S. W. First-principles Prediction of Thermodynamically Stable Two-Dimensional Electrides. *J. Am. Chem. Soc.* **2016**, *138*, 15336.

(171) Zhang, Y.; Wang, H.; Wang, Y.; Zhang, L.; Ma, Y. Computer-Assisted Inverse Design of Inorganic Electrides. *Phys. Rev. X* **2017**, *7*, 011017.

(172) Park, C.; Kim, S. W.; Yoon, M. First-Principles Prediction of New Electrides with Nontrivial Band Topology Based on One-Dimensional Building Blocks. *Phys. Rev. Lett.* **2018**, *120*, 026401.

(173) Zhang, X.; Guo, R.; Jin, L.; Dai, X.; Liu, G. Intermetallic Ca_3Pb: a topological zero-dimensional electride material. *J. Mater. Chem. C* **2018**, *6*, 575.

(174) MatNavi, NIMS Materials Database. "http://mits.nims.go.jp/index_en.html".

(175) Detemple, W. Inorganic Crystal Structure Database. "https://icsd.fiz-karlsruhe.de".

(176) Atoji, M.; Kikuchi, M. Crystal Structures of Cubic and Trigonal Yttrium Hypocarbides; A Dimorphically Interphased Single-Crystal Study. *J. Chem. Phys.* **1969**, *51*, 3863.

(177) Maehlen, J. P.; Yartys, V. A.; Hauback, B. C. Structural studies of deuterides of yttrium carbide. *J. Alloy. Compd.* **2003**, *351*, 151.

(178) Oh, J. S.; Kang, C.-J.; Kim, Y. J.; Sinn, S.; Han, M.; Chang, Y. J.; Kim, S. W.; Min, B. I.; Kim, H.-D.; Noh, T. W. Evidence for Anionic Excess Electrons in a Quasi-Two-Dimensional Ca_2N Electride by Angle-Resolved Photoemission Spectroscopy. *J. Am. Chem. Soc.* **2016**, *138*, 2496.

(179) Park, J.; Lee, K.; Lee, S. Y.; Nandadasa, C. N.; Kim, S.; Lee, K. H.; Lee, Y. H.; Hosono, H.; Kim, S.-G.; Kim, S. W. Strong localization of anionic electrons at interlayer for electrical and magnetic anisotropy in two-dimensional Y_2C electride. *J. Am. Chem. Soc.* **2017**, *139*, 615.

(180) Hu, J.; Xu, B.; Yang, S. A.; Guan, S.; Ouyang, C.; Yao, Y. 2D electrides as promising anode materials for Na-ion batteries from first-principles study. *ACS Appl. Mater. Interfaces* **2015**, *7*, 24016.

(181) Hou, J.; Tu, K.; Chen, Z. Two-Dimensional Y_2C Electride: A Promising Anode Material for Na-Ion Batteries. *J. Phys. Chem. C* **2016**, *120*, 18473.

(182) Kim, S.; Song, S.; Park, J.; Yu, H. S.; Cho, S.; Kim, D.; Baik, J.; Choe, D.-H.;

Chang, K. J.; Lee, Y. H.; Kim, S. W.; Yang, H. Long-Range Lattice Engineering of $MoTe_2$ by a 2D Electride. *Nano letters* **2017**, *17*, 3363–3368.

(183) Kim, Y. J.; Kim, S. M.; Yu, C.; Yoo, Y.; Cho, E. J.; Yang, J. W.; Kim, S. W. Chemoselective Hydrodehalogenation of Organic Halides Utilizing Two-Dimensional Anionic Electrons of Inorganic Electride $[Ca_2N]^+ \cdot e^-$. *Langmuir* **2017**, *33*, 954–958.

(184) Guan, S.; Huang, S. Y.; Yao, Y.; Yang, S. A. Tunable hyperbolic dispersion and negative refraction in natural electride materials. *Phys. Rev. B* **2017**, *95*, 165436.

(185) Cudazzo, P.; Gatti, M. Collective charge excitations of the two-dimensional electride Ca_2N. *Phys. Rev. B* **2017**, *96*, 125131.

(186) Yi, S.; Choi, J.-H.; Lee, K.; Kim, S. W.; Park, C. H.; Cho, J.-H. Stacking-sequence-independent band structure and shear exfoliation of two-dimensional electride materials. *Phys. Rev. B* **2016**, *94*, 235428.

(187) Dale, S. G.; Johnson, E. R. The ionic versus metallic nature of 2D electrides: a density-functional description. *Phys. Chem. Chem. Phys* **2017**, *19*, 27343.

(188) Park, J.; Hwang, J.-Y.; Lee, K. H.; Kim, S.-G.; Lee, K.; Kim, S. W. Tuning the spin-alignment of interstitial electrons in two-dimensional Y_2C electride via chemical pressure. *J. Am. Chem. Soc.* **2017**, *139*, 17277.

(189) Feng, C.; Shan, J.; Xu, A.; Xu, Y.; Zhang, M.; Lin, T. First-principle study of pressure-induced phase transitions and electronic properties of electride Y_2C. *Solid State Commun.* **2017**, *266*, 34–38.

(190) He, Y. The structural, electronic, elastic and thermodynamics properties of 2D transition-metal electride Y_2C via first-principles calculations. *J. Alloy. Compd.* **2016**, *654*, 180.

(191) Ge, Y.; Guan, S.; Liu, Y. Two dimensional superconductors in electrides. *New J. Phys.* **2017**, *19*, 123020.

(192) Huang, H.; Jin, K.; Zhang, S.; Liu, F. Topological Electride Y_2C. *Nano Lett.* **2018**, *18*, 1972.

(193) Druffel, D. L.; Kuntz, K. L.; Woomer, A. H.; Alcorn, F. M.; Hu, J.; Donley, C. L.; Warren, S. C. Experimental Demonstration of an Electride as a 2D Material. *J. Am. Chem. Soc.* **2016**, *138*, 16089.

(194) Zhao, S.; Li, Z.; Yang, J. Obtaining two-dimensional electron gas in free space without resorting to electron doping: an electride based design. *J. Am. Chem. Soc.* **2014**, *136*, 13313.

(195) Inoshita, T.; Takemoto, S.; Tada, T.; Hosono, H. Surface electron states on the quasi-two-dimensional excess-electron compounds Ca_2N and Y_2C. *Phys. Rev. B* **2017**, *95*, 165430.

(196) Oh, Y.; Lee, J.; Park, J.; Kwon, H.; Jeon, I.; Kim, S. W.; Kim, G.; Park, S.; Hwang, S. W. Electric field effect on the electronic structure of 2D Y_2C electride. *2D Mater.* **2018**, *5*, 035005.

(197) Sansom, J. E. H.; Richings, D.; Slater, P. R. A powder neutron diffraction study of the oxide-ion-conducting apatite-type phases, $La_{9.33}Si_6O_{26}$ and $La_8Sr_2Si_6O_{26}$. *Solid State Ionics* **2001**, *139*, 205.

(198) Chevalier, B.; Hermes, W.; Heying, B.; Rodewald, U. C.; Hammerschmidt, A.; Matar, S. F.; Gaudin, E.; Pottgen, R. New Hydrides REScSiH and REScGeH (RE= La, Ce): Structure, Magnetism, and Chemical Bonding. *Chem. Mater.* **2010**, *22*, 5013.

(199) Parthe, E. The crystal structure of Y_5Si_3 and Y_5Ge_3. *Acta Crystallogr.* **1960**, *13*, 868.

(200) Koch, C.; Scarbrough, J. Superconductivity in Mo-Re and Nb-Ir σ Phases. *Phys. Rev. B* **1971**, *3*, 742.

(201) Kobayashi, Y.; Kitano, M.; Kawamura, S.; Yokoyama, T.; Hosono, H. Kinetic evidence: the rate-determining step for ammonia synthesis over electride-supported Ru catalysts is no longer the nitrogen dissociation step. *Catal. Sci. Technol.* **2017**, *7*, 47–50.

(202) Li, Y.; Li, Z.-R.; Wu, D.; Li, R.-Y.; Hao, X.-Y.; Sun, C.-C. An ab initio prediction of the extraordinary static first hyperpolarizability for the electron-solvated cluster $(FH)_2e(HF)$. *J. Phys. Chem. B* **2004**, *108*, 3145.

(203) Chen, W.; Li, Z.-R.; Wu, D.; Gu, F.-L.; Hao, X.-Y.; Wang, B.-Q.; Li, R.-J.; Sun, C.-C. The static polarizability and first hyperpolarizability of the water trimer anion: ab initio study. *J. Chem. Phys.* **2004**, *121*, 10489.

(204) Chen, W.; Li, Z.-R.; Wu, D.; Li, Y.; Sun, C.-C.; Gu, F. L. The structure and the large nonlinear optical properties of Li@Calix[4]pyrrole. *J. Am. Chem. Soc.* **2005**, *127*, 10977.

(205) Chen, W.; Li, Z.-R.; Wu, D.; Li, Y.; Sun, C.-C.; Gu, F. L.; Aoki, Y. Nonlinear optical properties of alkalides Li^+(Calix[4]pyrrole)M^-(M= Li, Na, and K): alkali anion atomic number dependence. *J. Am. Chem. Soc.* **2006**, *128*, 1072.

(206) Jing, Y.-Q.; Li, Z.-R.; Wu, D.; Li, Y.; Wang, B.-Q.; Gu, F. L.; Aoki, Y. Effect of the Complexant Shape on the Large First Hyperpolarizability of Alkalides $Li^+(NH_3)_4M^-$. *ChemPhysChem* **2006**, *7*, 1759.

(207) Ma, F.; Li, Z.-R.; Xu, H.-L.; Li, Z.-J.; Li, Z.-S.; Aoki, Y.; Gu, F. L. Lithium Salt Electride with an Excess Electron Pair? A Class of Nonlinear Optical Molecules for Extraordinary First Hyperpolarizability. *J. Phys. Chem. A* **2008**, *112*, 11462.

(208) Wang, F.-F.; Li, Z.-R.; Wu, D.; Wang, B.-Q.; Li, Y.; Li, Z.-J.; Chen, W.; Yu, G.-T.; Gu, F. L.; Aoki, Y. Structures and Considerable Static First Hyperpolarizabilities: New Organic Alkalides ($M^+@n^6adz)M'^-$(M, M'= Li, Na, K; n= 2, 3) with Cation Inside and Anion Outside of the Cage Complexants. *J. Phys. Chem. B* **2008**, *112*, 1090.

(209) Li, Z.-J.; Li, Z.-R.; Wang, F.-F.; Luo, C.; Ma, F.; Wu, D.; Wang, Q.; Huang, X.-R. A dependence on the petal number of the static and dynamic first hyperpolarizability for electride molecules: many-petal-shaped Li-doped cyclic polyamines. *J. Phys. Chem. A* **2009**, *113*, 2961.

(210) Muhammad, S.; Xu, H.; Liao, Y.; Kan, Y.; Su, Z. Quantum mechanical design and structure of the $Li@B_{10}H_{14}$ basket with a remarkably enhanced electro-optical response. *J. Am. Chem. Soc.* **2009**, *131*, 11833.

(211) Liu, Z.-B.; Zhou, Z.-J.; Li, Y.; Li, Z.-R.; Wang, R.; Li, Q.-Z.; Li, Y.; Jia, F.-Y.; Wang, Y.-F.; Li, Z.-J.; Cheng, J.-B. Push–pull electron effects of the complexant in a Li atom doped molecule with electride character: a new strategy to enhance the first hyperpolarizability. *Phys. Chem. Chem. Phys.* **2010**, *12*, 10562.

(212) Xu, H.-L.; Wang, F.-F.; Chen, W.; Yu, G.-T. The complexant shape effect on first (hyper) polarizability of alkalides $Li^+(NH_2CH_3)_4M^-$(M= Li, Na, and K). *Int. J. Quantum Chem.* **2011**, *111*, 3174.

(213) Xu, H.-L.; Sun, S.-L.; Muhammad, S.; Su, Z.-M. Three-propeller-blade-shaped electride: remarkable alkali-metal-doped effect on the first hyperpolarizability. *Theor. Chem. Acc.* **2011**, *128*, 241.

(214) Zhou, Z.-J.; Li, H.; Huang, X.-R.; Wu, Z.-J.; Ma, F.; Li, Z.-R. The structure and large nonlinear optical properties of a novel octupolar electride $Li@3^6adz$. *Comp. Theor. Chem.* **2013**, *1023*, 99.

(215) Sun, W.-M.; Wu, D.; Li, Y.; Li, Z.-R. Theoretical study on superalkali (Li_3) in ammonia: novel alkalides with considerably large first hyperpolarizabilities. *Dalton T.* **2014**, *43*, 486.

(216) Sun, W.-M.; Fan, L.-T.; Li, Y.; Liu, J.-Y.; Wu, D.; Li, Z.-R. On the potential application of superalkali clusters in designing novel alkalides with large nonlinear optical properties. *Inorg. Chem.* **2014**, *53*, 6170.

(217) Srivastava, A. K.; Misra, N. Novel Li_3X_3 supersalts (X=F, Cl, Br and I) and their alkalide characteristics. *New J. Chem.* **2014**, *38*, 2890.

(218) Kumar, A.; Gadre, S. R. On the electrostatic nature of electrides. *Phys. Chem. Chem. Phys.* **2015**, *17*, 15030.

(219) Postils, V.; Garcia-Borràs, M.; Solà, M.; Luis, J. M.; Matito, E. On the existence and characterization of molecular electrides. *Chem. Comm.* **2015**, *51*, 4865.

(220) Wang, J.-J.; Zhou, Z.-J.; He, H.-M.; Wu, D.; Li, Y.; Li, Z.-R.; Zhang, H.-X. An External Electric Field Manipulated Second-Order Nonlinear Optical Switch of an Electride Molecule: A Long-Range Electron Transfer Forms a Lone Excess Electron Pair and Quenches Singlet Diradical. *J. Phys. Chem. C* **2016**, *120*, 13656.

(221) Sun, W.-M.; Li, X.-H.; Li, Y.; Ni, B.-L.; Chen, J.-H.; Li, C.-Y.; Wu, D.; Li, Z.-R. Theoretical Study of the Substituent Effect on the Nonlinear Optical Properties of a Room-temperature Stable Organic Electride. *ChemPhysChem* **2016**, *17*, 3907.

(222) El Bakouri, O.; Postils, V.; Garcia-Borràs, M.; Duran, M.; Luis, J. M.; Calvello, S.; Soncini, A.; Matito, E.; Feixas, F.; Solà, M. Metal Cluster Electrides: a new Type of Molecular Electrides with Delocalised Polyattractor Character. *Chem. Eur. J.* **2018**, *24*, 9853.

(223) Goodarzi, M.; Nazari, F.; Illas, F. Electronic and structural properties of Li_n@ Be_2B_8 (n= 1–14) and Li_n@ Be_2B_{36} (n= 1–21) nanoflakes shed light on possible anode materials for Li-based batteries. *J. Comp. Chem.* **2018**, *39*, 1795.

(224) Blanchard-Desce, M.; Alain, V.; Bedworth, P.; Marder, S.; Fort, A.; Runser, C.; Barzoukas, M.; Lebus, S.; Wortmann, R. Large quadratic hyperpolarizabilities with donor–acceptor polyenes exhibiting optimum bond length alternation: correlation between structure and hyperpolarizability. *Chem. Eur. J.* **1997**, *3*, 1091.

Graphical TOC Entry